

# Lepton flavor violating Higgs boson decays from massive seesaw neutrinos

Ernesto Arganda, Ana M. Curiel<sup>y</sup> and María J. Herrero<sup>z</sup>

Dpto. de Física Teórica, Universidad Autónoma de Madrid, Spain.

David Temes<sup>x</sup>

Laboratoire de Physique Théorique, LAPTH, France<sup>1</sup>.

## Abstract

Lepton flavor violating Higgs boson decays are studied within the context of seesaw models with Majorana massive neutrinos. Two models are considered: The SM seesaw, with the Standard Model particle content plus three right handed neutrinos, and the MSSM seesaw, with the minimal Supersymmetric Standard Model particle content plus three right handed neutrinos and their supersymmetric partners. The widths for these decays are derived from a full one-loop diagrammatic computation in both models, and they are analyzed numerically in terms of the seesaw parameters, namely, the Dirac and Majorana masses. Several possible scenarios for these masses that are compatible with neutrino data are considered. In the SM seesaw case, very small branching ratios are found for all studied scenarios. These ratios are explained as a consequence of the decoupling behaviour of the heavy right handed neutrinos. In contrast, in the MSSM seesaw case, sizeable branching ratios are found for some of the leptonic flavor violating decays of the MSSM neutral Higgs bosons and for some choices of the seesaw masses and MSSM parameters. The relevance of the two competing sources of lepton flavor changing interactions in the MSSM seesaw case is also discussed. The non-decoupling behaviour of the supersymmetric particles contributing in the loop-diagrams is finally shown.

PACS numbers:

---

<sup>1</sup>URA 14-36 du CNRS, associée à l'Université de Savoie  
Electronic address: ernesto.arganda@uam.es

<sup>y</sup>Electronic address: ana.curie@uam.es

<sup>z</sup>Electronic address: maria.herrero@uam.es

<sup>x</sup>Electronic address: temes@lapp.in2p3.fr

## I. INTRODUCTION

The present strong evidence for lepton flavor changing neutrino oscillations [1] in solar and atmospheric neutrino data, as well as in the KamLAND reactor experiment, implies the existence of non-zero masses for the light neutrinos, and provides the first experimental clue for physics beyond the Standard Model (SM). The experimentally suggested smallness of the neutrino masses can be explained in a very simple and elegant way by the seesaw mechanism of neutrino mass generation [2]. This mechanism requires the introduction of heavy right-handed (RH) Majorana neutrinos which are singlet under the SM gauge symmetry group and whose Majorana masses,  $m_M$ , can therefore be much higher than the SM particle masses. In this context, the smallness of the light left-handed (LH) neutrino masses appears naturally due to the induced large suppression by the ratio of the two very distant mass scales that are involved in the seesaw mass matrices, the Majorana matrix  $m_M$  and the Dirac matrix  $m_D$ . The latter is generated after electroweak symmetry breaking by  $m_D = Y \langle H \rangle$ , where  $Y$  is the Yukawa matrix for couplings between the RH and LH neutrinos, and  $\langle H \rangle = v = 174$  GeV is the SM Higgs boson vacuum expectation value. For the one generation case, and assuming a Yukawa coupling of order one, the suggested small neutrino mass value signals towards a new physics mass scale of the order of  $m_M = 10^{14}$  GeV, but the pattern and size of the seesaw mass parameters can vary much respect to this in the most general case of three generations.

Another appealing feature of the seesaw models is that the RH Majorana neutrinos can successfully generate, through their CP-violating decays and via leptogenesis, the observed baryon asymmetry of the Universe. There is, however, one negative aspect in the standard version of the seesaw models. It is that the presence of the two distant mass scales can lead to a severe hierarchy problem, and this requires the introduction of supersymmetry (SUSY) to be solved. In the SUSY-seesaw models, the hierarchy between  $m_M$  and the electroweak scale is stabilized by the new contributions of the SUSY partners of the RH and LH neutrinos. Thus, the SUSY-seesaw models, and particularly the simplest version given by the Minimal Supersymmetric Standard Model (MSSM), are becoming more popular.

One of the most interesting features of the SUSY-seesaw models is the associated rich phenomenology due to the occurrence of lepton flavor violating (LFV) processes. Whereas in the standard (non-SUSY) seesaw models the ratios of LFV processes are small due to

the smallness of the light neutrino masses, in the SU SY -seesaw models these can be large due to an important additional source of lepton flavor mixing in the soft-SU SY breaking terms. Even in the scenarios with universal soft-SU SY breaking parameters at the large energy scale associated to the SU SY breaking  $M_X$  (which could be the Planck mass, the SU SY -GUT mass or something else, but always well above  $m_M$ ), the running from this scale down to  $m_M$  induces, via the neutrino Yukawa couplings, large lepton flavor mixing in the slepton soft masses, and provides the so-called slepton-lepton misalignment, which in turn generates non-diagonal lepton flavor interactions. These interactions can induce sizable ratios in several LFV processes with SM charged leptons in the external legs, which are actually being tested experimentally with high precision and therefore provide a very interesting window to look for indirect SU SY signals.

In addition to the previously mentioned radiatively induced LFV effect, there is another source of radiative LFV effects in the M SSM -seesaw, which is generated from the neutrino sector mixing. Namely, the off-diagonal entries of the Maki-Nakagawa-Sakata (MNS) matrix,  $U_{MNS}$  [3], produce lepton flavor non-diagonal interactions, this time involving exclusively charge currents which can also generate, via loops, important contributions to the mentioned LFV processes with SM charged leptons in the external legs. In the M SSM -seesaw, these LFV effects from neutrino mixing could indeed compete with the other source from slepton-lepton misalignment, providing interesting consequences, as will be shown here. This competitiveness of the two flavor changing sources has indeed been noticed previously in the squark sector, concretely in the SU SY electroweak one-loop contributions to flavor changing Higgs boson decays,  $h^0 \rightarrow b\bar{b}; s\bar{s}$  [4]. Interestingly, the lepton sector will manifest more evidently these competing effects than the quark sector, since the MNS matrix being preferred by neutrino data is clearly non-diagonal, whereas the CKM matrix is close to the identity matrix.

Among the various LFV processes that have been considered in the literature, the most fruitfull ones are the radiative  $\gamma \rightarrow e^+ e^-$ ,  $\gamma \rightarrow \mu^+ \mu^-$ , and  $\gamma \rightarrow \tau^+ \tau^-$  decays, since their branching ratios are tested with high precision [5, 6, 7]. These usually provide the most restrictive experimental bounds on the M SSM -seesaw parameters. Another interesting LFV decays include rare decays, Z boson decays  $Z \rightarrow l^+ l^-$  and Higgs boson decays  $H \rightarrow l^+ l^-$ , with  $k \in m$ .

We are interested here in the LFV Higgs boson decays (LFVHD),  $H \rightarrow e^+ e^-$ ,  $H \rightarrow \mu^+ \mu^-$ ,

and the branching ratios that can be generated in the context of the seesaw models with parameters being compatible with the neutrino data and the most relevant data of and radiative decays. In this work we consider both versions of the seesaw mechanism for neutrino mass generation: the SM -seesaw and the M SSM -seesaw. In the first one, the SM particle content is enlarged by three singlet RH Majorana neutrinos, and in the second one, the M SSM particle content is enlarged by three singlet RH Majorana neutrinos and their corresponding SUSY partners. We present here a complete one-loop computation of the LFVHD widths in both seesaw scenarios and analyze the size of the associated branching ratios in terms of the seesaw parameters. In order to make contact between the seesaw mass matrices and the experimental neutrino data, we use the general parametrization introduced in ref. [8], where the Yukawa neutrino couplings, and therefore  $m_D$ , are expressed in terms of the three physical light neutrino masses,  $m_i$ , the three physical heavy neutrino masses,  $m_{N_i}$ , the  $U_{MNS}$  matrix, and a general complex  $3 \times 3$  orthogonal matrix  $R$ .

The LFVHD within the SM -seesaw was studied some time ago in ref. [9]. There, it was considered a very specific seesaw scenario where all the light neutrinos were exactly massless at tree level [10] and the Dirac mass was taken very large. The conclusion was that branching ratios for  $H_{SM} \rightarrow \nu \bar{\nu}$  decays as large as  $10^{-4} - 10^{-5}$  can be achieved for  $m_{H_{SM}} = 140$  GeV. Besides, these ratios were found to grow with the heavy neutrino masses, and this growing suggested a non-decoupling behaviour of the heavy neutrinos. The crucial assumption for that behaviour was to take very large  $m_D$  values, which implied very strong neutrino Yukawa couplings. Here, we have recalculated the LFVHD rates in the complete one-loop diagrammatic approach and updated the numerical estimates in the light of the recent neutrino data, by fixing the input parameters  $m_i$  and  $U_{MNS}$  to their data preferred values. We then make our estimates for specific choices of the input unknown parameters,  $m_{N_i}$  and  $R$  and pay special attention to those which generate successful baryon asymmetry. For all the studied cases we find ratios that are many orders of magnitude smaller than in ref. [9]. The reason for these small ratios is because the heavy RH neutrinos do indeed decouple in our SM -seesaw scenario and our assumptions for the seesaw parameters do not imply large  $m_D$  values. For completeness, we also include in this part, an estimate of the LFVHD rates in the case of Dirac massive neutrinos and compare them with the previous estimate of ref. [11].

The second part of this work concerns with the evaluation of the LFVHD ratios in the

context of the M SSM -seesaw. Concretely,  $h^0; H^0; A^0 \rightarrow l_k l_n$ , with  $k \neq n$ . The subject of LFV HD being generated from loops of SUSY particles has been considered previously in refs. [11] and [12]. In ref. [11] it was analyzed a specific SUSY-SU(5) scenario where the slepton-lepton mass misalignment was generated exclusively from the running of the trilinear A-terms. On the other hand, the computation of ref. [12] was not in the context of the M SSM -seesaw but in a more generic scenario for slepton-lepton mass misalignment and they did not include the lepton flavor violating source from the neutrino mixing. Besides, in ref. [12], the effective lagrangian approach that is valid for large  $\tan \beta$  values and large SUSY mass values is used. We present here instead, a complete one-loop computation in the M SSM -seesaw context and do not rely on any of the above approximations. We include in the computation both sources of lepton flavor violating interactions, the slepton-lepton mass misalignment and the neutrino mixing via  $U_{MNS}$ . The slepton-lepton mass misalignment is generated, as it is usual in the seesaw models, by the renormalization group running of the slepton soft parameters from the high energies  $M_X$  down to  $m_M$ . The diagonalization of the generated slepton mass matrix is then performed. That is, we do not rely on either the mass insertion approximation or the large  $\tan \beta$  effective lagrangian approach and, therefore, our results are valid for all  $\tan \beta$  values and all soft-SUSY-breaking mass values. We will explore the size of the branching ratios for the Higgs decays as a function of the relevant M SSM parameters, which within the context of mSUGRA are the universal soft masses  $M_0, M_{1-2}$  and  $\tan \beta$ , and of the relevant seesaw parameters, which are  $m_{N_1}$  and the R matrix. We will analyze in parallel the branching ratios for the  $l_j \neq l_i$  decays as a function of the same parameters. The requirement of compatibility with the present data on  $l_j \neq l_i$  decays, mainly  $l_j \neq e$ , will provide us with the maximum allowed ratios for the Higgs decays. We will also study the behaviour of the LFV HD widths in the limit of very heavy SUSY masses and will find that the sleptons, sneutrinos, charginos and neutralinos do not decouple in this observable. For large SUSY masses, large  $\tan \beta$ , particular choices of the see-saw parameters and by ignoring the effects from  $U_{MNS}$ , we will find agreement with the numerical results of ref. [12].

The paper is organized as follows. Section II contains a short summary of the mass parameters and mixings in the neutrino sector of the seesaw models. The relation between these parameters and the experimental neutrino masses and mixings is also included. Section III is devoted to the computation and analysis of the LFV HD rates in the context of the

SM -seesaw. The decoupling behaviour of the heavy neutrinos is also studied in this section. Section IV starts by presenting the two sources of LFV interactions in the context of the MSSM -seesaw. Next the computation and analysis of the LFVHD rates within that context is included. The non-decoupling behaviour of the SUSY particles in the LFVHD widths is studied at the end of this section. Section V is devoted to the conclusions.

## II. NEUTRINO MASSES AND MIXINGS IN THE SEESAW MODELS

In this section and in order to fix our notation we briefly review the mass parameters and mixings in the neutrino sector of the seesaw models and relate them to the physical light neutrino masses and neutrino mixing angles which are extracted from neutrino data. We follow closely here and in the next sections the notation of refs. [9, 10] for SM -seesaw and ref. [8] for SUSY -seesaw and for the connection with neutrino data.

We start with the Yukawa-sector of the SM -seesaw that contains the three LH SM neutrinos  $\overset{0}{\nu}_L$  and three extra RH massive neutrinos  $\overset{0}{\nu}_R$ , whose Yukawa interactions provide, after spontaneous electroweak symmetry breaking, the following mass Lagrangian containing the Dirac and Majorana mass terms,

$$L_{\text{mass}} = \frac{1}{2} \begin{pmatrix} 0 & 1 \\ \overset{0}{\nu}_L & (\overset{0}{\nu}_R)^C \end{pmatrix} M \begin{pmatrix} 0 & 1 \\ \overset{0}{\nu}_R & \overset{0}{\nu}_L \end{pmatrix} A + h.c.; \quad (1)$$

where,

$$M = \begin{pmatrix} 0 & 1 \\ 0 & m_D \\ m_D^T & m_M \end{pmatrix} A; \quad (2)$$

Here  $m_D$  is the 3 × 3 Dirac mass matrix that is related to the 3 × 3 Yukawa coupling matrix  $Y$  and the SM Higgs vacuum expectation value,  $\langle H \rangle = v = 174 \text{ GeV}$ , by  $m_D = Y \langle H \rangle$ ; and  $m_M$  is the 3 × 3 Majorana mass matrix for the RH massive neutrinos that is real, non singular and symmetric.

The mass matrix  $M$  is a 6 × 6 complex symmetric matrix that can be diagonalized by a 6 × 6 unitary matrix  $U$  in the following way:

$$U^T M U = \hat{M} = \text{diag}(m_1; m_2; m_3; m_{N_1}; m_{N_2}; m_{N_3}); \quad (3)$$

This gives 3 light Majorana neutrino mass eigenstates  $\nu_i$ , with masses  $m_i$  ( $i = 1, 2, 3$ ), and

three heavy ones  $N_i$ , with masses  $m_{N_i}$  ( $i=1,2,3$ ), which are related to the weak eigenstates via,

$$\begin{matrix} 0 & 1 \\ @ & \begin{pmatrix} 0 \\ L \end{pmatrix} \\ \begin{pmatrix} 0 \\ R \end{pmatrix}^C \end{matrix} A = U \begin{matrix} 0 & 1 \\ @ & L \\ N_L \end{matrix} \quad \text{and} \quad \begin{matrix} 0 & 1 \\ @ & \begin{pmatrix} 0 \\ L \end{pmatrix}^C \\ \begin{pmatrix} 0 \\ R \end{pmatrix} \end{matrix} A = U \begin{matrix} 0 & 1 \\ @ & R \\ N_R \end{matrix} : \quad (4)$$

The seesaw mechanism for neutrino mass generation assumes a large separation between the two mass scales involved in  $m_D$  and  $m_M$  matrices. More specifically, we shall assume here that all matrix elements of  $m_D$  are much smaller than those of  $m_M$ ,  $m_D \ll m_M$ , and we will perform an analytical expansion of all relevant parameters and observables in power series of a matrix defined as,

$$m_D m_M^{-1} : \quad (5)$$

In particular, the previous diagonalization of the mass matrix  $M$  can be solved in power series of [13]. For simplicity, we choose to work here and in the rest of this paper, in a basis where the Right Hand Majorana mass matrix,  $m_M$ , and the charged lepton mass matrix,  $M^1$ , are avor diagonal. This means that all avor mixing of the light sector is included in the mixing matrix  $U_{MNS}$ . By working to the lowest orders of these power series expansions one finds, in the avor basis, the following neutrino 3 3 matrices,

$$\begin{aligned} m &= m_D^T + O(m_D^{-3})' \quad m_D m_M^{-1} m_D^T \\ m_N &= m_M + O(m_D^{-1})' \quad m_M : \end{aligned} \quad (6)$$

Here,  $m_N$  is already diagonal, but  $m$  is not yet diagonal. The rotation from this avor basis to the mass eigenstate basis is finally given by the MNS unitary matrix,  $U_{MNS}$ . Thus,

$$\begin{aligned} m^{\text{diag}} &= U_{MNS}^T m U_{MNS} = \text{diag}(m_1; m_2; m_3); \\ m_N^{\text{diag}} &= m_N = \text{diag}(m_{N1}; m_{N2}; m_{N3}); \end{aligned} \quad (7)$$

and the diagonalization of  $M$  in eqs. (2) and (3) can be performed by the following unitary 6 6 matrix:

$$U = @ \begin{pmatrix} 0 & & & & & 1 \\ (1 & \frac{1}{2} & & & & \\ & & T & & & \\ & & & (1 & \frac{1}{2} & T \\ & & & & & \\ & & & T & (1 & \frac{1}{2} & T \\ & & & & & & \\ & & & & & & \end{pmatrix} A + O(4): \quad (8)$$

As for the  $U_{MNS}$  matrix, we use the standard parametrization given by,

$$U_{MNS} = \begin{pmatrix} 0 & & & 1 \\ \begin{matrix} B \\ \bar{B} \\ \bar{C} \\ \bar{C} \end{matrix} & \begin{matrix} c_{12}c_{13} & & & \\ s_{12}c_{13} & s_{12}s_{23}s_{13}e^i & c_{12}c_{23} & s_{12}s_{23}s_{13}e^i \\ s_{12}c_{23} & c_{12}s_{23}s_{13}e^i & c_{12}s_{23} & s_{12}c_{23}s_{13}e^i \\ s_{12}s_{23} & c_{12}c_{23}s_{13}e^i & c_{12}s_{23} & c_{23}c_{13} \end{matrix} & \begin{matrix} s_{13}e^i \\ c_{13} \\ s_{23}c_{13} \\ c_{23}c_{13} \end{matrix} \end{pmatrix} \text{diag}(1; e^i; e^i); \quad (9)$$

where  $c_{ij} = \cos \theta_{ij}$  and  $s_{ij} = \sin \theta_{ij}$ .

Finally, in order to make contact with the experimental data, we use the method proposed in ref [8]. It provides a simple way to reconstruct the Dirac mass matrix by starting with the physical light and heavy neutrino masses, the  $U_{MNS}$  matrix, and a general complex and orthogonal matrix  $R$ . With our signs and matrix conventions this relation can be written as,

$$m_D^T = \text{diag}(1; 1; 1) R m^{\text{diag}} U_{MNS}^+ \quad (10)$$

where,  $R^T R = 1$ . Thus, instead of proposing directly possible textures for  $m_D$ , one proposes possible values for  $m_{N_1}; m_{N_2}; m_{N_3}$  and  $R$ , and sets  $m_1; m_2; m_3$  and  $U_{MNS}$  to their suggested values from the experimental data. Notice that any hypothesis for  $R$  different from the unit matrix will lead to an additional lepton flavor mixing between the LH and RH neutrino sectors. Notice that, to be strict, the previous relation holds at the energy scale  $m_M$ , and to use it properly one should use the RGE to run the input experimental data  $m^{\text{diag}}$  and  $U_{MNS}$  from the low energies up to  $m_M$ . However these effects are tiny and will be ignored here.

For the numerical estimates in this paper we will consider the following two plausible scenarios being compatible with data:

Scenario A : quasi-degenerate light and degenerate heavy neutrinos,

$$m_1 = 0.2 \text{ eV}; m_2 = m_1 + \frac{m_{\text{sol}}^2}{2m_1}; m_3 = m_1 + \frac{m_{\text{atm}}^2}{2m_1}; \quad (11)$$

$$m_{N_1} = m_{N_2} = m_{N_3} = m_N$$

Scenario B : hierarchical light and hierarchical heavy neutrinos,

$$m_1 = 0 \text{ eV}; m_2 = \frac{q}{m_{\text{sol}}^2}; m_3 = \frac{p}{m_{\text{atm}}^2}; \quad (12)$$

$$m_{N_1} < m_{N_2} < m_{N_3}$$

In the two above scenarios, we will fix the input data to the following values,  $\frac{p}{m^2_{sol}} = 0.008 \text{ eV}$ ,  $\frac{p}{m^2_{atm}} = 0.05 \text{ eV}$ ,  $_{12} = _{sol} = 30^\circ$ ,  $_{23} = _{atm} = 45^\circ$ ,  $_{13} = 0^\circ$  and  $= = = 0$  (See for instance, ref. [14]).

Regarding the matrix  $R$ , we will consider correspondingly one of the following three cases:

### Case 0

$$R = R_0 = 1 \quad (13)$$

This is a reference case which is chosen here just because it is the simplest possibility.

### Case 1

$$R = R_1 = \begin{matrix} 0 & & & & & 1 \\ \begin{matrix} C_2 C_3 & C_1 S_3 & S_1 S_2 C_3 & S_1 S_3 & C_1 S_2 C_3 \\ \begin{matrix} \text{B} \\ \text{B} \\ \text{B} \\ \text{B} \\ \text{B} \end{matrix} & \begin{matrix} C_1 S_3 \\ C_2 S_3 \\ C_1 C_3 \\ S_1 S_2 S_3 \\ S_1 C_3 \end{matrix} & \begin{matrix} S_1 S_2 C_3 \\ S_1 S_3 \\ S_1 C_3 \\ C_1 S_2 S_3 \\ C_1 C_2 \end{matrix} & \begin{matrix} S_1 S_3 \\ S_1 C_3 \\ C_1 S_2 S_3 \\ C_1 C_2 \end{matrix} & \begin{matrix} C \\ C \\ C \\ C \\ A \end{matrix} \end{matrix} : \quad (14)$$

where  $c_i = \cos \theta_i$ ,  $s_i = \sin \theta_i$  and  $\theta_1, \theta_2$  and  $\theta_3$  are arbitrary complex angles. This parametrization was proposed in ref. [8] for the study of  $\pi^+ \rightarrow e^+ \nu_e$  decays. It has also been considered in ref. [15] with specific values for the  $\theta_i$  angles to study the implications for baryogenesis in the case of hierarchical neutrinos.

### Case 2

$$R = R_2 = e^{iA} O; \quad (15)$$

with  $0 = 1$ , and

$$A = \begin{pmatrix} 0 & a & b \\ a & 0 & c \\ b & c & 0 \end{pmatrix} : \quad (16)$$

Here,  $a$ ,  $b$ , and  $c$  are three real parameters that are constrained by perturbativity of the Yukawa couplings. In particular, for  $a = b = c = k$  and  $m_{1,2,3} = 0.2 \text{ eV}$ , it leads to  $k < (1.4; 0.9; 0.3)$  for  $m_{1,2,3} = (10^{10}; 10^{12}; 10^{14}) \text{ GeV}$  respectively. This choice has been proven in ref. [16] to provide successful baryon asymmetry via leptogenesis for the case of quasi-degenerate neutrinos, and still provide branching ratios for  $\bar{\nu}_j \rightarrow \bar{\nu}_i + (i \neq j)$  rare decays which are compatible with data.

All that has been summarized in this section applies to the MSSM seesaw model as well. The only difference is that in this case,  $m_D$  is related to one of the two Higgs vacuum expectation values by  $m_D = Y \langle H_2 \rangle$ , where  $\langle H_2 \rangle = v_2 = v \sin \theta$ .

### III. LEPTON FLAVOUR VIOLATION IN Higgs Decays in the SM -SEESAW

In this section we compute and analize the LFVHD widths,  $(H \rightarrow l_k l_m)$  with  $k \neq m$ , within the context of the SM -seesaw with three RH neutrinos which has been shortly reviewed in the previous section. The branching ratios for these decays were studied some time ago in ref. [9] in a particular scenario of the SM -seesaw where all the light neutrino masses were exactly zero at the tree level and the Dirac mass was taken very large. The small masses for the light neutrinos were then generated by the one-loop electroweak radiative corrections [10]. Besides, the numerical results of ref. [9] for the case of 3 generations were obtained under particular approximations for the evaluation of the one-loop diagrams, as for instance,  $m_{l_1} = 0$ ,  $\frac{m_{l_2}^2}{m_W^2} \ll 1$ ,  $\frac{m_H^2}{4m_W^2} \ll 1$ , the latter being nowadays clearly not a very good approximation given the present lower bound on  $m_H$  from LEP of about 115 GeV. Here we have recomputed these LFVHD widths for all the channels and we have included all contributing one-loop diagrams without assuming any approximation. One of the main points of our analysis is the update of the numerical results by taking into account the present experimental neutrino data. In addition we will reanalyze the behaviour of these partial widths with the large heavy neutrino masses. In contrast to ref. [9], where the important enhancement of the widths found with  $m_{N_i}$  suggested a non-decoupling behaviour of the heavy neutrinos, we will find instead a clear decoupling behaviour. The main difference between ref. [9] and us is the assumption on  $m_D$ , which in their work was taken very large (therefore, leading to strong neutrino Yukawa couplings), whereas in our case the assumptions for the input  $m_{N_i}$  and  $R$ , do not lead to large  $m_D$ .

We start by writing down the interactions that are relevant for the computation of the LFVHD widths to one-loop and in the mass eigenstate basis. Denoting the Majorana neutrino mass eigenstates collectively by  $n_i$  (i.e.,  $n_i = n_i$  for  $i = 1, 2, 3$  and  $n_i = N_{i+3}$  for  $i = 4, 5, 6$ ), the relevant interactions between  $n_i$  and  $W^+$ ,  $H$  and the Goldstone bosons  $G$  can be written respectively as follows,

$$\begin{aligned}
 L_{\text{int}}^W &= \frac{g}{2} \bar{W} \gamma_5 B \bar{n}_j P_L n_j + h.c; \\
 L_{\text{int}}^H &= \frac{g}{4m_W} \bar{H} n_i (m_{n_i} + m_{n_j}) \text{Re}(C_{n_i n_j}) + i \frac{g}{4m_W} (m_{n_j} - m_{n_i}) \text{Im}(C_{n_i n_j}) n_j; \\
 L_{\text{int}}^G &= \frac{g}{2m_W} \bar{G} \gamma_5 B \bar{n}_j (m_{l_k} P_L - m_{n_j} P_R) n_j + h.c
 \end{aligned} \tag{17}$$

where, the coupling factors  $B_{1n_j}$  ( $i=1,2,3, j=1,..6$ ) and  $C_{n_i n_j}$  ( $i,j=1,..6$ ) are defined in terms of the  $U$  matrix of eq. 3 by:

$$B_{1n_j} = U_{ij} \quad (18)$$

$$C_{n_i n_j} = \sum_{k=1}^{X^3} U_{ki} U_{kj} \quad (19)$$

Notice that our particular choice of diagonal charged leptons in the flavor basis is equivalent to assume a  $V$  matrix in [9] equal to the identity matrix. The expansions of these coupling matrices in power series of the  $U$  matrix can be easily derived from the expansion of  $U$  in eq. 8. For brevity, we omit here the indices and use a self-explanatory short notation. They are given by,

$$B_{ln} = (B_1; B_{ln}); \quad (20)$$

$$C_{nn} = \begin{matrix} 0 & 1 \\ @ & C & C_N \\ C_N & C_{NN} \end{matrix} A : \quad (21)$$

where,

$$\begin{aligned} B_1 &= (1 - \frac{1}{2} \gamma^+) U_{MNS} + O(\gamma^4) \\ B_{ln} &= (1 - \frac{1}{2} \gamma^+) + O(\gamma^5) \\ C &= U_{MNS}^T (1 - \gamma^+) U_{MNS} + O(\gamma^4) \\ C_N &= C_N^+ = U_{MNS}^T (1 - \gamma^+) + O(\gamma^5) \\ C_{NN} &= \gamma^+ + O(\gamma^4); \end{aligned} \quad (22)$$

After the computation of the 10 contributing one-loop diagrams, drawn in fig. 1, we find the analytical results presented in Appendix A which have been written in terms of the standard one-loop integrals,  $C_0; B_0; C_{12}; \dots$  etc, whose definitions can be found for instance in [17]. These provide the total contributions to the relevant form factors  $F_L$  and  $F_R$  that are related to the decay amplitude  $F$  by:

$$iF = -ig u_k (p_2) (F_L P_L + F_R P_R) v_{l_n} (p_3) \quad (23)$$

where,

$$F_L = \frac{X^{10}}{\sum_{i=1}^{10} F_L^{(i)}}; F_R = \frac{X^{10}}{\sum_{i=1}^{10} F_R^{(i)}} \quad (24)$$

and  $p_1 = p_3$   $p_2$  is the ingoing Higgs boson momentum.

The LFVHD widths can be obtained finally from these form factors by:

$$(H \rightarrow l_k l_n) = \frac{g^2}{16 m_H} \frac{v_u}{t} \frac{u_u}{1} \frac{m_{l_k} + m_{l_n}}{m_H} \frac{2!}{1} \frac{m_{l_k} m_{l_n}}{m_H} \frac{2!}{1} \dots \\ : (m_H^2 - m_{l_k}^2 - m_{l_n}^2) (F_L^2 + F_R^2) - 4 m_{l_k} m_{l_n} \text{Re}(F_L F_R) \quad (25)$$

Notice that since we will consider complex R matrices, the corresponding decay widths for the CP conjugate states, in general, can be different. We do not study here these CP conjugate decays and concentrate on the  $H \rightarrow l_k l_n$  decays.

Regarding the analytical results, it is worth mentioning that we have checked the finiteness of the total form factors  $F_L$  and  $F_R$ . When summing up all involved indices in each diagram, we find out, in agreement with ref. [9], that the only divergent diagrams left are 1, 8 and 10 and these divergences cancel among each other, providing the expected finite result.

We next present the numerical results. The one-loop functions  $C_0, B_0, \dots$  have been evaluated with the Mathematica package of [18]. For the numerical estimates of the branching ratios we evaluate the coupling matrices of eq. 22 in terms of  $\lambda$ , for the particular input values of  $m_D$  and  $m_M$  that are compatible with the neutrino data. That is, we get  $m_D$  from eq. 10, for the two scenarios A and B and for various choices of the input masses  $m_{N_{1,2,3}}$  and the matrix  $R$ , as explained in sec. II, and take  $m_{M_i} = m_{N_i}$ . The total width has been evaluated with the HDECAY program me [19].

The main conclusion from the results in table I is that the LFVHD rates in the SM - seesaw are extremely small and depend strongly on the Majorana mass scale. In all scenarios considered here and for large  $m_N$ , say larger than  $10^4$  GeV, the decay rates decrease with the Majorana mass, as  $(1-m_M^2)$ , and therefore they become very small for very large masses of the heavy neutrinos. This behaviour is easily explained by the fact that the dominant contributions to the form factors are proportional to  $(m_D^2 - m_M^2)$  and,  $m_D$  being obtained by eq. 10 goes as  $m_D \propto m_M^{1/2}$ , so that the form factors scale as  $F \propto 1/m_M$  and, consequently, the branching ratios as  $B \propto 1/m_M^2$ . That is, we get decoupling of the heavy neutrinos. We have checked numerically this behaviour, as can be seen in fig 2. Incidentally,

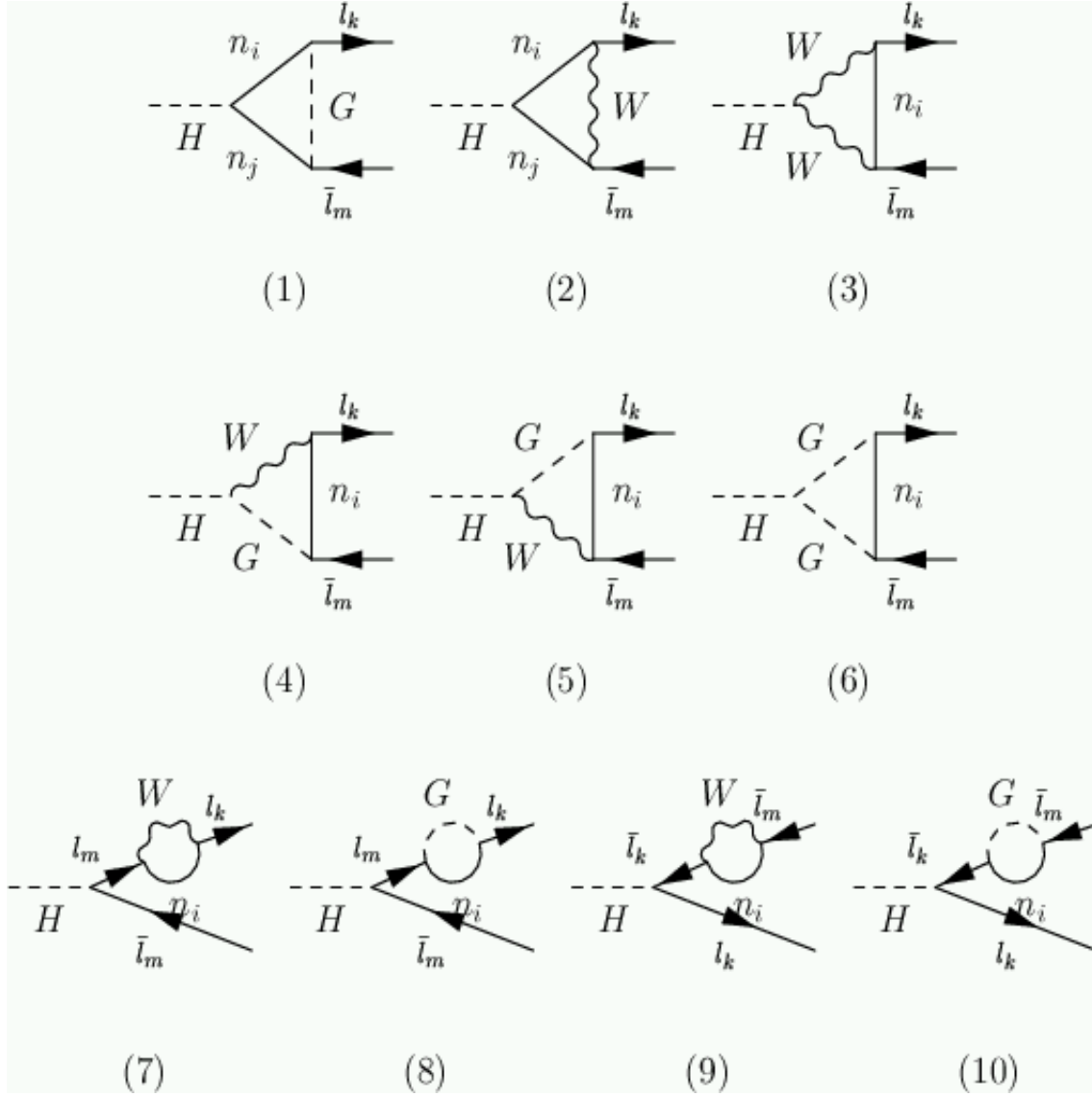


FIG. 1: One-loop diagrams for LFV HD in the SM seesaw model

It should be mentioned that since we are keeping the masses of the light neutrinos non-vanishing, the asymptotic value is not exactly zero but an extremely small value.

The  $R$  matrix that appears in the relation between  $m_D$  and  $m_M$  can be also relevant in some scenarios. In particular, if the  $\theta_i$  angles are complex, the  $R$ -matrix elements can have large modulus, the derived  $m_D$  can increase relevantly and, therefore, the decay rates can be much larger, although still very small. This can be seen clearly by comparing the first and second columns of table I. Notice also that, due to the leptonic mass hierarchy, the larger rates are always obtained for the decays involving the  $e$ -lepton.

Therefore one can conclude that the LFV HD rates in the SM seesaw are negligibly small

		R <sub>0</sub>		R <sub>1</sub>	
(A) $m_{N_{1,2,3}} = 10^3$ GeV	B R <sub>12</sub>	3	$10^{42}$	2	$10^{32}$
	B R <sub>13</sub>	1	$10^{39}$	2	$10^{30}$
	B R <sub>23</sub>	3	$10^{36}$	3	$10^{30}$
(A) $m_{N_{1,2,3}} = 10^6$ GeV	B R <sub>12</sub>	1	$10^{46}$	1	$10^{36}$
	B R <sub>13</sub>	3	$10^{44}$	1	$10^{34}$
	B R <sub>23</sub>	1	$10^{40}$	1	$10^{34}$
(B) $m_{N_{1(2)}} = 1(5) \cdot 10^3$ GeV $m_{N_3} = 1 \cdot 10^5$ GeV	B R <sub>12</sub>	1	$10^{38}$	1	$10^{35}$
	B R <sub>13</sub>	1	$10^{36}$	3	$10^{33}$
	B R <sub>23</sub>	1	$10^{37}$	3	$10^{32}$
(B) $m_{N_{1(2)}} = 1(5) \cdot 10^4$ GeV $m_{N_3} = 1 \cdot 10^6$ GeV	B R <sub>12</sub>	4	$10^{39}$	1	$10^{36}$
	B R <sub>13</sub>	1	$10^{37}$	1	$10^{34}$
	B R <sub>23</sub>	1	$10^{37}$	2	$10^{33}$

TABLE I: Branching ratios of the LFVHD in the SM seesaw, for scenarios A and B and for various choices of the heavy neutrino masses. The R matrix is chosen as in case 0 and case 1 with  $m_{1,2,3} = 3e^{i\pi/3}$ . Here,  $B R_{12} = B R(H \rightarrow e)$ ,  $B R_{13} = B R(H \rightarrow e)$ ,  $B R_{23} = B R(H \rightarrow \nu)$  and  $m_H = 115$  GeV.

and the largest values are for the lowest Majorana mass choices and largest complex angles in the R matrix. These conclusions are valid for both scenarios A and B.

In order to compare these results with the ones obtained in [9], it has to be taken into account that in their computation the seesaw parameter was fixed to a particular numerical value, so that, for large  $m_M$ ,  $m_D$  scales as  $m_D \sim m_M$ , in contrast to our case where, as we have said,  $m_D \sim m_M^{1/2}$ . These different assumptions on the relation between  $m_D$  and  $m_M$  give rise to very different decay rates. The branching ratios in their computation grow instead with  $m_M$ , thus by providing very large values to the Dirac masses (i.e., the Yukawa couplings get strong as  $m_N$  (i.e.,  $m_M$  increases) they obtained much larger values for the branching ratios. For a fixed neutrino mass  $m_N$ , the only way to reach these large values for the Dirac masses in our scenario is by considering extremely large complex R-matrix elements. As an example, in scenario A and case 1 with  $M_{N_i} = 1$  TeV and  $m_{1,2,3} = 5i$ ,

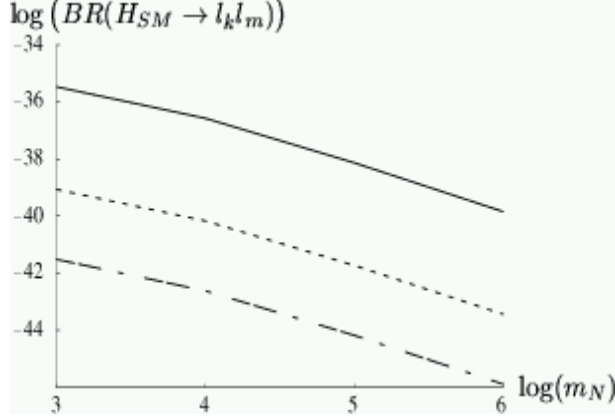


FIG. 2: Dependence of the LFV HD ratios in the SM seesaw with  $m_N$  (GeV) in scenario A with degenerate neutrinos. Solid, short-dashed and long-dashed lines are for  $BR_{23}$ ;  $BR_{13}$  and  $BR_{12}$  respectively.

we obtain  $m_D \approx 200$  GeV and  $BR_{23} \approx 10^{-6}$ , which are closer to the predicted values in ref. [9]. But this is not a natural assumption in seesaw models since it requires a strong fine-tuning in the choice of the  $m_D$  and  $m_M$  matrices.

We also include next, for comparison, the numerical results for the LFV HD branching ratios in the case of Dirac neutrinos and for  $m_H = 115$  GeV. For the two scenarios A and B they are, correspondingly:

$$\begin{aligned}
 BR(H \rightarrow e) &= 2 \cdot 10^{-62} \text{ (A)}; 2 \cdot 10^{-62} \text{ (B)} \\
 BR(H \rightarrow e) &= 1 \cdot 10^{-60} \text{ (A)}; 1 \cdot 10^{-60} \text{ (B)} \\
 BR(H \rightarrow \nu) &= 3 \cdot 10^{-56} \text{ (A)}; 2 \cdot 10^{-56} \text{ (B)}
 \end{aligned}$$

As we can see, these ratios are negligible and much smaller than in the case of Majorana neutrinos. We also learn from our results that the ratios undergo a strong cancellation when the internal neutrinos in the loop diagrams are summed over the three generations. This suppression is similar to the GIM suppression mechanism of the quark sector. Notice that our rates disagree in many orders of magnitude with the results of ref. [11], where a prediction of  $BR(H \rightarrow \nu) \approx 6 \cdot 10^{-7}$  was presented. We believe that this disagreement could be due to the above mentioned strong cancellations which are not taking place in their case.

## IV . LEPTON FLAVOR VIOLATING HIGGS DECAYS IN THE M SSM -SEESAW

In this section we study the lepton flavor violating Higgs decays within the context of the M SSM -seesaw model. We first analyze the various sources of lepton flavor changing processes in this model, and next we compute the LFVHD partial widths and branching ratios for the three neutral M SSM Higgs boson decays,  $(H_x \rightarrow l_1 l_2)$  with  $H_x = h_0; H_0; A_0$  and  $l_1, l_2 = e, \mu, \tau$ .

### A . Sources of LFV interactions in the M SSM -seesaw

In the M SSM -seesaw model there are two sources of lepton flavor changing processes. The first one is induced from the non-vanishing mixing in the light neutrino sector, that is from the off-diagonal elements of the  $U_{MNS}$  matrix. We have already seen in the previous section that these elements induce, via charged currents, intergenerational interactions of the type,  $W \bar{l}_i l_j$  (and the corresponding  $G \bar{l}_i l_j$ ) with  $i \neq j$ . These will be generated in the M SSM -seesaw as well, but in addition, there will appear new LFV interactions involving charginos,  $\tilde{\chi}^\pm$ , charged sleptons,  $\tilde{l}$  and sneutrinos,  $\tilde{\nu}$ , as for instance,  $W \bar{l}_i \tilde{\chi}_j^\pm$ ,  $W \bar{\tilde{l}}_i l_j$  and  $W \bar{\tilde{\chi}}_i^\pm \tilde{\chi}_j^\pm$  with  $i \neq j$ . From the operational point of view, these effects are introduced by the explicit factors of the  $U_{MNS}$  matrix elements in the corresponding couplings when referred to the physical basis. Thus, for instance, in the simplest case where the charged sleptons rotate parallelly to the charged leptons, and the sneutrinos rotate parallelly to the neutrinos, the  $W \bar{l}_i \tilde{\chi}_j^\pm$ ,  $W \bar{\tilde{l}}_i l_j$ , and  $W \bar{\tilde{\chi}}_i^\pm \tilde{\chi}_j^\pm$  couplings will get a  $(U_{MNS})_{ij}$  factor in the same way as the  $W \bar{l}_i l_j$  coupling does. Due to the extended Higgs sector of the M SSM -seesaw, there will be additional intergenerational couplings of the type,  $H \bar{l}_i l_j$  and  $H \bar{\tilde{l}}_i \tilde{\chi}_j^\pm$  with similar  $(U_{MNS})_{ij}$  factors.

All the previous intergenerational couplings can induce, via radiative corrections, important contributions to LFV processes. In the following we will refer to these radiatively induced flavor changing effects from the  $(U_{MNS})_{ij}$  factors in the couplings as  $U_{MNS}$  effects. For the case under study here of LFVHD, the couplings inducing these  $U_{MNS}$  effects are  $W \bar{l}_i l_j$ ,  $H \bar{l}_i l_j$  and  $\tilde{\chi}_i^\pm \bar{l}_j$ . The size of the generated effects from the  $W \bar{l}_i l_j$  couplings are expected to be as small as in the SM -seesaw case. The only difference comes from the different couplings of the internal particles to the external  $h_0; H_0$ , and  $A_0$  Higgs bosons as

compared to those of the SM Higgs boson  $H$ , but this difference will not change relevantly the small size of the generated ratios. On the other hand, the generated effects from the  $H \tilde{l}_i \tilde{l}_j$  couplings are new with respect to the SM seesaw case. We have numerically estimated the size of the contributions to the LFV HD branching ratios from all the one-loop diagrams with internal  $H$ ,  $W$  and  $G$ , and we have found that they are indeed always negligibly small. We will in consequence ignore all these contributions in the following and keep just the contributions from the  $\sim \tilde{l}_i \tilde{l}_j$  couplings.

The second source of LFV processes in the MSSM seesaw is genuine in SUSY models and comes from the misalignment between the rotations leading to the mass eigenstate basis of sleptons relatively to that of leptons. This misalignment is radiatively generated in the SUSY seesaw models from the Yukawa couplings of the Majorana neutrinos and can be sizeable in both the charged slepton and sneutrino sectors. Once one rotates the so-generated flavor non-diagonal charged slepton and sneutrino mass matrices to the physical diagonal ones, some intergenerational couplings involving SUSY particles are generated again. For the case of LFV HD, the involved couplings are  $\sim \tilde{l}_i \tilde{l}_j$  and  $\sim^0 \tilde{l}_i \tilde{l}_j$  with  $i \neq j$ . These generated effects from lepton-slepton misalignment will be called in the following misalignment effects. By considering both the  $U_{MNS}$  and the misalignment effects together, the  $\sim \tilde{l}_i \tilde{l}_j$  couplings will get in the physical basis both the  $U_{MNS}$  factors and the corresponding matrix rotation factors from misalignment, whereas the  $\sim^0 \tilde{l}_i \tilde{l}_j$  couplings will get just the later ones. All these couplings will induce via loops of SUSY particles relevant contributions to the LFV HD rates as will be shown later on.

The LFV effects from misalignment are usually implemented in the seesaw models in the language of the Renormalization Group Equations (RGE) and can be summarized as follows. One starts with universal soft-SUSY-breaking parameters at the large energies  $M_X \gg m_M$  given by,

$$(m_L)_{ij}^2 = M_0^2 \tilde{m}_{ij}; (m_E)_{ij}^2 = M_0^2 \tilde{m}_{ij}; (m_{M'})_{ij}^2 = M_0^2 \tilde{m}_{ij}; (A_L)_{ij} = A_0 (Y_L)_{ij}; (A_E)_{ij} = A_0 (Y_E)_{ij} \quad (26)$$

where,  $M_0$  and  $A_0$  are the universal soft-slepton mass and soft-trilinear coupling respectively.  $Y_L$  is the Yukawa coupling matrix of the charged leptons, which is flavor diagonal in the basis chosen here,  $(Y_L)_{ij} = Y_{\tilde{l}_i} \tilde{m}_{ij}$  with  $Y_{\tilde{l}_i} = \frac{m_{\tilde{l}_i}}{v_1}$  and  $v_1 = v \cos \theta$ .  $Y_E$  is the Yukawa coupling matrix of the neutrinos and is given by,  $(Y_E)_{ij} = \frac{(m_{M'})_{ij}}{v_2}$ , with  $v_2 = v \sin \theta$ .

The effect of the RGE running from  $M_X$  down to  $m_M$  on the off-diagonal soft parameters

of the charged slepton sector, to one-loop and in the leading-log approximation, is then described by,

$$\begin{aligned}
 (m_L^2)_{ij} &= \frac{1}{8^2} (3M_0^2 + A_0^2) (Y_L Y^T)_{ij} \\
 (A_1)_{ij} &= \frac{3}{16^2} A_0 Y_{1i} (Y_L Y^T)_{ij} \\
 (m_E^2)_{ij} &= 0; L_{kl} \log \frac{M_X}{m_{M_k}} \quad \text{for } k \neq l
 \end{aligned} \tag{27}$$

Notice that our notation is slightly different from the usual one in that  $Y_L \neq Y^T$ . For all the numerical estimates in this work we use  $M_X = 2 \times 10^{16}$  GeV and, for simplicity, we will assume  $A_0 = 0$ . Thus, we only consider flavor changing in the LL sector, which is known to be a very good approximation. In fact, we have checked that even for values as large as  $A_0 = M_0 = 1$  TeV the size of the corresponding flavor changing dimensionless parameters in the LR sector are always smaller than the LL ones in more than three orders of magnitude. Notice also that, in addition to the previously mentioned  $U_{MNS}$  factors in the  $\sim l_i \sim l_j$  couplings, there is an extra dependence on  $U_{MNS}$  via the  $Y$  couplings or, equivalently, via the  $m_D$  matrix as given in eq. 10. Thus, even if we fix  $U_{MNS}$  to the unit matrix, there could be still flavor changing effects from misalignment via the  $R$  matrix. Conversely, if we fix  $R$  to the unit matrix, there could be still flavor changing effects from the  $U_{MNS}$  matrix, coming from both the  $U_{MNS}$  factors in the couplings and the  $U_{MNS}$  in  $m_D$ . Finally, notice that the effect of neutrino Yukawa couplings, via RG evolution from  $M_X$  down to  $m_M$ , on the diagonal entries of the squared-mass matrices are small, and have been neglected in this work.

In order to illustrate the size of the misalignment effects, we show in fig. (3) the predictions for the flavor changing dimensionless parameter, in the LL sector, defined as  $\frac{(m_L^2)_{ij}}{M_0^2}$ , as a function of the seesaw parameters, and in some selected examples within the scenarios described before. We show in fig. (3a) the dependence of  $_{ij}$  with  $m_N$ , for scenario A and real  $R$ . Notice that in this scenario with degenerate  $m_{N_i}$ , the  $_{ij}$  are independent on  $R$ , so this figure applies both to case 0 and to case 1 with  $i$  real. As can be seen, the three  $_{ij}$  are negative and the largest one, which is  $_{23}$ , reaches values up to  $2 \times 10^{-3}$  for  $m_N = 10^{14}$  GeV. The size of  $_{12}$  and  $_{13}$  is very similar (they are undistinguishable in this plot) and can reach values up to  $3 \times 10^{-5}$  for  $m_N = 10^{14}$  GeV. The size of the  $_{ij}$  in this scenario with degenerate heavy neutrinos can obviously be increased if  $R$  is assumed instead to be

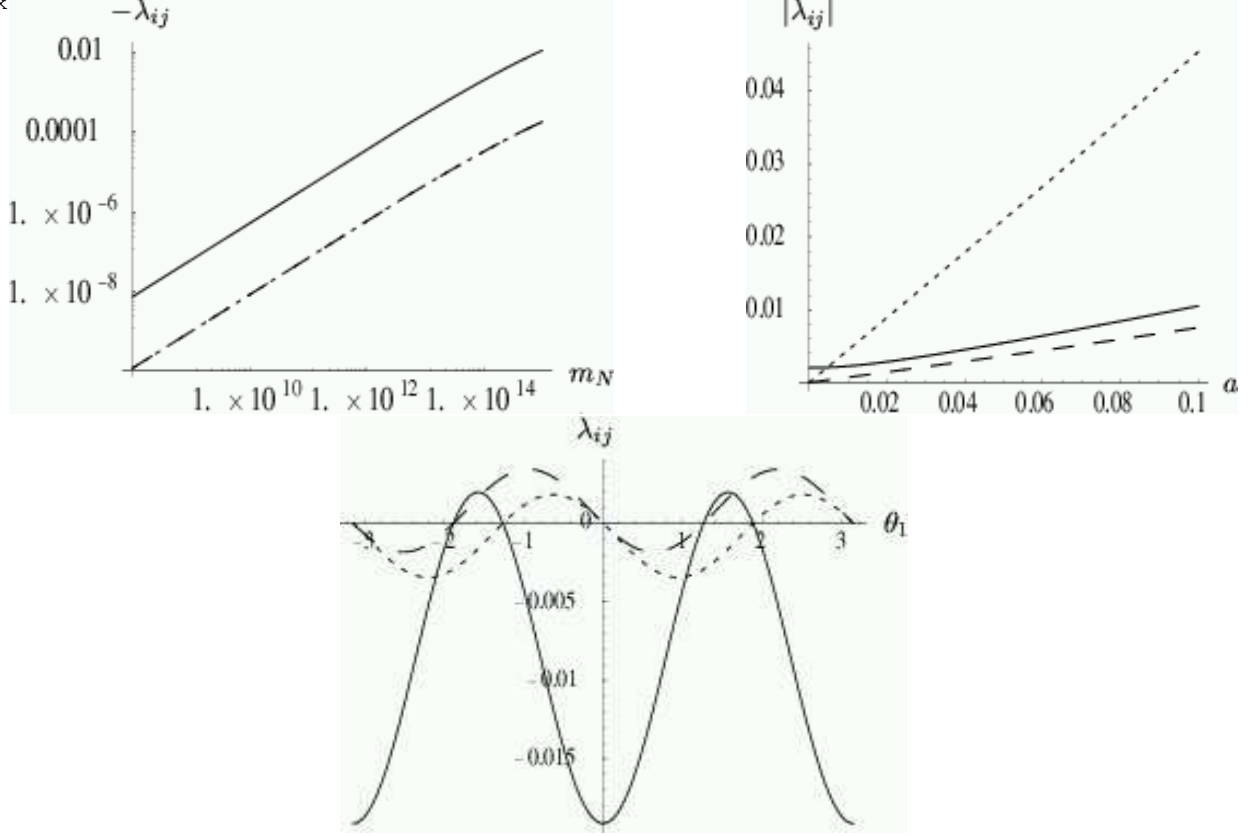


FIG. 3: Dependence of  $\lambda_{ij}$  with the seesaw parameters. Solid, long-dashed and short-dashed lines are for  $\lambda_{23}$ ,  $\lambda_{13}$  and  $\lambda_{12}$  respectively. (3a) Upper left panel: Dependence with  $m_N$  in scenario A for R real. (3b) Upper right panel: Dependence with the  $a$  parameter in scenario A with  $m_N = 10^{14}$  GeV and R complex, for case 2 with  $a = b = c$ . (3c) Lower panel: Dependence with real  $\theta_1$  in scenario B, case 1, for  $(m_{N_1}; m_{N_2}; m_{N_3}) = (10^8; 2 \times 10^8; 10^{14})$  GeV and  $\theta_2 = \theta_3 = 0$ .

complex. In this case, the  $\lambda_{ij}$  are in general complex numbers. As an example, we show in fig. (3b) the dependence of  $\lambda_{ij}$ , in scenario A with  $m_N = 10^{14}$  GeV, on the parameter  $a$  of case 2, for  $a = b = c$ . The size of  $\lambda_{ij}$  increases clearly with  $a$  and, for the studied range,  $|\lambda_{12}|$  can be as large as  $4.5 \times 10^{-2}$ . In particular, for values of  $a$  between  $10^{-5}$ , that generate successful baryogenesis [16], the generated  $\lambda_{ij}$  are still large, mainly  $|\lambda_{12}| = 10^{-2}$ . Notice also that the relative size of the different  $\lambda_{ij}$  changes respect to fig. (3a). The case of hierarchical neutrinos is shown in fig. (3c), where it is plotted the dependence with  $\theta_1$  for scenario B with  $(m_{N_1}; m_{N_2}; m_{N_3}) = (10^8; 2 \times 10^8; 10^{14})$  GeV and real R, with  $\theta_2 = \theta_3 = 0$ . We see that  $\lambda_{23}$  is the largest one and reaches values up to  $0.02$  at  $\theta_1 = 0$ .

The next step is the diagonalization of the charged slepton and sneutrino mass matrices

leading to the mass eigenvalues and mass eigenstates at the electroweak energy scale. We start with the non-diagonal charged slepton and sneutrino squared-mass matrices that are obtained after the running from  $M_X$  to  $M_W$  and once the charged leptons and neutrinos have been rotated to the physical basis. For the charged sector, this matrix is referred to the  $(e_L; e_R; \tilde{e}_L; \tilde{e}_R; \tilde{\nu}_L; \tilde{\nu}_R)$  basis and can be written as follows,

$$M_I^2 = \begin{pmatrix} 0 & & & & & & 1 \\ M_{LL}^{ee2} & M_{LR}^{ee2} & M_{LL}^{e2} & 0 & M_{LL}^{e2} & 0 & C \\ M_{RL}^{ee2} & M_{RR}^{ee2} & 0 & 0 & 0 & 0 & C \\ M_{LL}^{e2} & 0 & M_{LL}^{2} & M_{LR}^{2} & M_{LL}^{2} & 0 & C \\ 0 & 0 & M_{RL}^{2} & M_{RR}^{2} & 0 & 0 & C \\ M_{LL}^{e2} & 0 & M_{LL}^{2} & 0 & M_{LL}^{2} M_{LR}^{2} & A \\ 0 & 0 & 0 & 0 & M_{RL}^{2} M_{RR}^{2} & A \end{pmatrix} \quad (28)$$

where,

$$\begin{aligned} M_{LL}^{112} &= m_{E;1}^2 + m_1^2 + m_z^2 \cos 2 \left( \frac{1}{2} + \sin \frac{\theta_w}{2} \right) \\ M_{RR}^{112} &= m_{E;1}^2 + m_1^2 - m_z^2 \cos 2 \sin \frac{\theta_w}{2} \\ M_{LR}^{112} &= M_{RL}^{112} = m_1 (A_1 - \tan \theta_w) \\ M_{LL}^{e2} &= (m_{E;1}^2)_{12}; M_{LL}^{e2} = (m_{E;1}^2)_{21} \\ M_{LL}^{e2} &= (m_{E;1}^2)_{13}; M_{LL}^{e2} = (m_{E;1}^2)_{31} \\ M_{LL}^{e2} &= (m_{E;1}^2)_{23}; M_{LL}^{e2} = (m_{E;1}^2)_{32}; \end{aligned} \quad (29)$$

The soft SUSY breaking masses and trilinear couplings above,  $m_{E;1}$ ,  $m_{E;1}$ ,  $m_{E;1}$ , and  $A_1$ , refer to their corresponding values at the electroweak scale. We got them by solving numerically the RGE with the program mSUSPECT [20] and by imposing the universality conditions at  $M_X = 2 \times 10^{16}$  GeV for the sfermion sector, eq. 26, together with the corresponding ones for the gaugino and Higgs boson sectors,  $M_1(M_X) = M_2(M_X) = M_{1=2}$  and  $M_{H_1}(M_X) = M_{H_2}(M_X) = M_0$  respectively. For the gaugino sector, this implies the well known relation at low energies,  $M_1(M_W) = \frac{5}{3} (\tan \theta_w)^2 M_2(M_W)$ . The value of the supersymmetric parameter is extracted as usual from the electroweak breaking condition. We choose in all this paper,  $\mu > 0$ , and do not expect relevant differences for  $\mu < 0$ .

After diagonalization of the  $M_I^2$  matrix one gets the physical slepton masses and the

six mass eigenstates  $(\tilde{\chi}_1^0, \dots, \tilde{\chi}_6^0)$   $\tilde{\chi}^0$  which are related to the previous weak eigenstates  $(\tilde{\chi}_L^0, \dots, \tilde{\chi}_R^0)$   $\tilde{\chi}$  by the corresponding  $6 \times 6$  rotation matrix,  $\tilde{\chi}^0 = R^{(1)} \tilde{\chi}$ .

Regarding the sneutrino sector one proceeds similarly to the charged slepton sector, but now the diagonalization process is simpler because of the involved seesaw matrix which gives rise naturally to a suppression of the R H sneutrino components in the relevant mass eigenstates. This can be easily illustrated in the one generation case, but for three generations one arrives to similar conclusions. The sneutrino mass terms of the MSSM seesaw model can be written in the one generation case [21],

$$L_{\text{mass}} = \text{Re}(\tilde{\chi}_L) \text{Re}(\tilde{\chi}_R) \text{Im}(\tilde{\chi}_L) \text{Im}(\tilde{\chi}_R) \begin{pmatrix} 0 & 1 & 0 & 1 \\ 0 & 0 & \text{Re}(\tilde{\chi}_L) & \text{Re}(\tilde{\chi}_R) \\ 0 & \text{M}_+^2 & 0 & \text{A} \\ 0 & \text{M}_-^2 & \text{A} & \text{Im}(\tilde{\chi}_L) \\ 0 & \text{M}_-^2 & \text{B} & \text{Im}(\tilde{\chi}_R) \end{pmatrix} \quad (30)$$

with,

$$\text{M}^2 = \begin{pmatrix} 0 & 1 \\ \text{m}_L^2 + \text{m}_D & \frac{1}{2}\text{m}_Z^2 \cos 2\theta \\ \text{m}_D(\text{A} - \cot \text{m}_M) & \text{m}_M^2 + \text{m}_D^2 + \text{m}_M^2 - 2\text{B}_M \text{m}_M \end{pmatrix} \quad (31)$$

Notice that now there are several mass scales involved, the soft SUSY breaking parameters,  $\text{m}_L$ ,  $\text{m}_M$ ,  $\text{B}_M$  and  $\text{A}$ , the Dirac mass  $\text{m}_D$ , the mass parameter, the Z boson mass  $\text{m}_Z$  and the Majorana neutrino mass  $\text{m}_M$ . Our basic assumption in all this paper is that  $\text{m}_M$  is much heavier than the other mass scales involved (obviously, except  $\text{M}_X$ ),  $\text{m}_M \gg \text{m}_D, \text{m}_Z, \text{m}_L, \text{m}_M, \text{A}, \text{B}_M$ . The size of  $\text{B}_M$  has been discussed in the literature [21] and seems more controversial. For simplicity, we shall assume here this is also smaller than  $\text{m}_M$ . In this situation, the diagonalization of the previous sneutrino squared mass matrix is simpler and leads to four mass eigenstates, two of which are light,  $\frac{1}{1}, \frac{1}{2}$  and two heavy,  $\frac{h}{1}, \frac{h}{2}$ . In the leading orders of the series expansion in powers of the mass eigenstates and their corresponding mass eigenvalues are given by,

$$\begin{aligned} \frac{1}{1} &= \frac{p}{2} (\text{Re}(\tilde{\chi}_L) - \text{Re}(\tilde{\chi}_R)) ; \frac{1}{2} = \frac{p}{2} (\text{Im}(\tilde{\chi}_L) - \text{Im}(\tilde{\chi}_R)) \\ \frac{h}{1} &= \frac{p}{2} (\text{Re}(\tilde{\chi}_R) + \text{Re}(\tilde{\chi}_L)) ; \frac{h}{2} = \frac{p}{2} (\text{Im}(\tilde{\chi}_R) + \text{Im}(\tilde{\chi}_L)) \\ \text{m}_{\frac{1}{1,2}}^2 &= \text{m}_L^2 + \frac{1}{2}\text{m}_Z^2 \cos 2\theta - 2\text{m}_D(\text{A} - \cot \text{B}_N) \\ \text{m}_{\frac{h}{1,2}}^2 &= \text{m}_M^2 - 2\text{B}_M \text{m}_M + \text{m}_M^2 + 2\text{m}_D^2 \end{aligned} \quad (32)$$

Here we can see that the heavy states  $h_{1,2}$  will couple very weakly to the rest of particles of the MSSM via their  $\tilde{\chi}_L$  component, which is highly suppressed by the small factor  $\epsilon$  and, therefore, it is a good approximation to ignore them and keep just the light states  $\tilde{\chi}_{1,2}^0$ , which are made mainly of  $\tilde{\chi}_L$  and its complex conjugate  $\tilde{\chi}_R$ . Now, by working in this simplified basis but applied to the three generations case, which we write for short  $\tilde{\chi}^0$  ( $i = 1, 2, 3$ ), the relevant 3 × 3 sneutrino squared mass matrix can be written as follows,

$$M_{\tilde{\chi}}^2 = \begin{matrix} 0 & & & 1 \\ \begin{matrix} \begin{matrix} B \\ \overline{B} \\ \overline{C} \end{matrix} & \begin{matrix} m_{\tilde{\chi}_1}^2 + \frac{1}{2}m_{\tilde{\chi}_2}^2 \cos 2 \\ (m_{\tilde{\chi}_1}^2)_{21} \\ (m_{\tilde{\chi}_1}^2)_{31} \end{matrix} & \begin{matrix} (m_{\tilde{\chi}_1}^2)_{12} \\ m_{\tilde{\chi}_2}^2 + \frac{1}{2}m_{\tilde{\chi}_1}^2 \cos 2 \\ (m_{\tilde{\chi}_2}^2)_{32} \end{matrix} & \begin{matrix} (m_{\tilde{\chi}_1}^2)_{13} \\ (m_{\tilde{\chi}_2}^2)_{23} \\ m_{\tilde{\chi}_3}^2 + \frac{1}{2}m_{\tilde{\chi}_1}^2 \cos 2 \end{matrix} \end{matrix} & C \\ \begin{matrix} \overline{B} \\ \overline{C} \\ \overline{A} \end{matrix} & \end{matrix} \quad (33)$$

where  $m_{\tilde{\chi}_1}^2$ , and  $(m_{\tilde{\chi}_i}^2)_{ij}$  are the same as in the previous charged slepton squared mass matrix. After diagonalization of the  $M_{\tilde{\chi}}^2$  matrix one gets the relevant physical sneutrino masses and eigenstates,  $\tilde{\chi}^0$  ( $i = 1, 2, 3$ ) which are related to the previous states  $\tilde{\chi}^0$  by the corresponding 3 × 3 rotation matrix,  $\tilde{\chi}^0 = R^{(i)} \tilde{\chi}^0$ .

To end up this subsection, we summarize all the interaction terms that are relevant for the computation of the LFV HD rates. We present these interactions in the physical mass eigenstate basis and will perform all the computations in this basis. It implies diagonalization in all the involved SUSY sectors, charged sleptons, sneutrinos, charginos, neutralinos and Higgs bosons. The SUSY-electroweak interaction terms among charginos, leptons and sneutrinos and among neutralinos, leptons and sleptons, that are the responsible for the LFV HD are as follows,

$$\begin{aligned} L_{\tilde{\chi}_j \tilde{\chi}^0} &= g_L^h A_L^{(1)} \tilde{\chi}_j P_L + A_R^{(1)} \tilde{\chi}_j P_R \tilde{\chi}_j^0 + h.c.; \\ L_{\tilde{\chi}_a \tilde{\chi}^0} &= g_L^h B_L^{(1)} \tilde{\chi}_a P_L + B_R^{(1)} \tilde{\chi}_a P_R \tilde{\chi}_a^0 + h.c.; \end{aligned} \quad (34)$$

where the coupling factors  $A_L^{(1)}$ ,  $A_R^{(1)}$ ,  $B_L^{(1)}$ , and  $B_R^{(1)}$  are given in Appendix B. Notice that the  $A$  factors contain the two announced sources of flavor changing, as can be noticed by the explicit  $U_{MN}$  and  $R^{(i)}$  matrices.

The other interaction terms which are not of lepton-flavor changing type, but enter in the computation of the LFV HD rates are the Higgs-lepton-lepton, Higgs-sneutrino-sneutrino, Higgs-slepton-slepton, Higgs-chargino-chargino, and Higgs-neutralino-neutralino interactions.

tions, reading:

$$\begin{aligned}
 L_{H_x ll} &= \frac{h}{gH_x l} S_{L;l}^{(x)} P_L + S_{R;l}^{(x)} P_R \frac{i}{l}; \\
 L_{H_x s s} &= \frac{iH_x}{h} g_{H_x \sim \sim} \sim \sim + g_{H_x l l} \frac{i}{l} \frac{i}{l}; \\
 L_{H_x \sim_i \sim_j} &= \frac{g}{h} H_x \sim_i W_{Lij}^{(x)} P_L + W_{Rij}^{(x)} P_R \frac{i}{l} \sim_j; \\
 L_{H_x \sim_a^0 \sim_b^0} &= \frac{g}{2} H_x \sim_a^0 D_{Lab}^{(x)} P_L + D_{Rab}^{(x)} P_R \frac{i}{l} \sim_b^0;
 \end{aligned} \tag{35}$$

where the coupling factors  $S_{L;q}^{(x)}$ ,  $S_{R;q}^{(x)}$ ,  $g_{H_x \sim \sim}$ ,  $g_{H_x l l}$ ,  $W_{Lij}^{(x)}$ ,  $W_{Rij}^{(x)}$ ,  $D_{Lab}^{(x)}$ , and  $D_{Rab}^{(x)}$  are collected in Appendix B.

## B . LFV HD rates in the M SSM -seesaw

As we have said, the contributions to the LFV HD rates in the M SSM -seesaw come from various sectors. The contributions from the charged Higgs sector and from the SM sector (ie,  $H^+$ ,  $W$  and  $G$ ) are very small and will not be included here. The main contributions come from the genuine SUSY sector, concretely, from the one-loop diagrams with charginos, neutralinos, sleptons and sneutrinos shown in fig. 4.

The contributions of these one-loop diagrams to the form factors are given by,

$$F_{L,x} = \sum_{i=1}^{X^8} F_{L,x}^{(i)}; \quad F_{R,x} = \sum_{i=1}^{X^8} F_{R,x}^{(i)}; \tag{36}$$

where the analytical results for  $F_{L,x}^{(i)}$  and  $F_{R,x}^{(i)}$ ,  $i = 1:8$ , are collected in Appendix B.

The partial widths for the  $h^0; H^0; A^0 \rightarrow l_1 l_2$  decays are then finally computed by inserting these form factors correspondingly into eq. 25. We show in figs. 5 to 11 the numerical results of the branching ratios for the LFV HD in the M SSM. The total M SSM Higgs boson widths have been computed with the HDECAY programme [19]. For the plots, we have selected the channels that illustrate the main points of our results, but in the discussion we will comment on all the channels. Similarly, for the comparison with the leptonic radiative decays,  $l_j \rightarrow l_i$ , we will show in the plots the most relevant one,  $e \rightarrow e$ , but we will also include in the discussion the comparison with the other decays. For the numerical estimates of the  $l_j \rightarrow l_i$  branching ratios we use the analytical formulas of ref. [22]. These are expressed in the mass eigenstate basis as well, and contain all contributing one-loop diagrams. For the involved  $l \sim$  and  $l^0 l^0$  couplings we use our expressions of Appendix B.

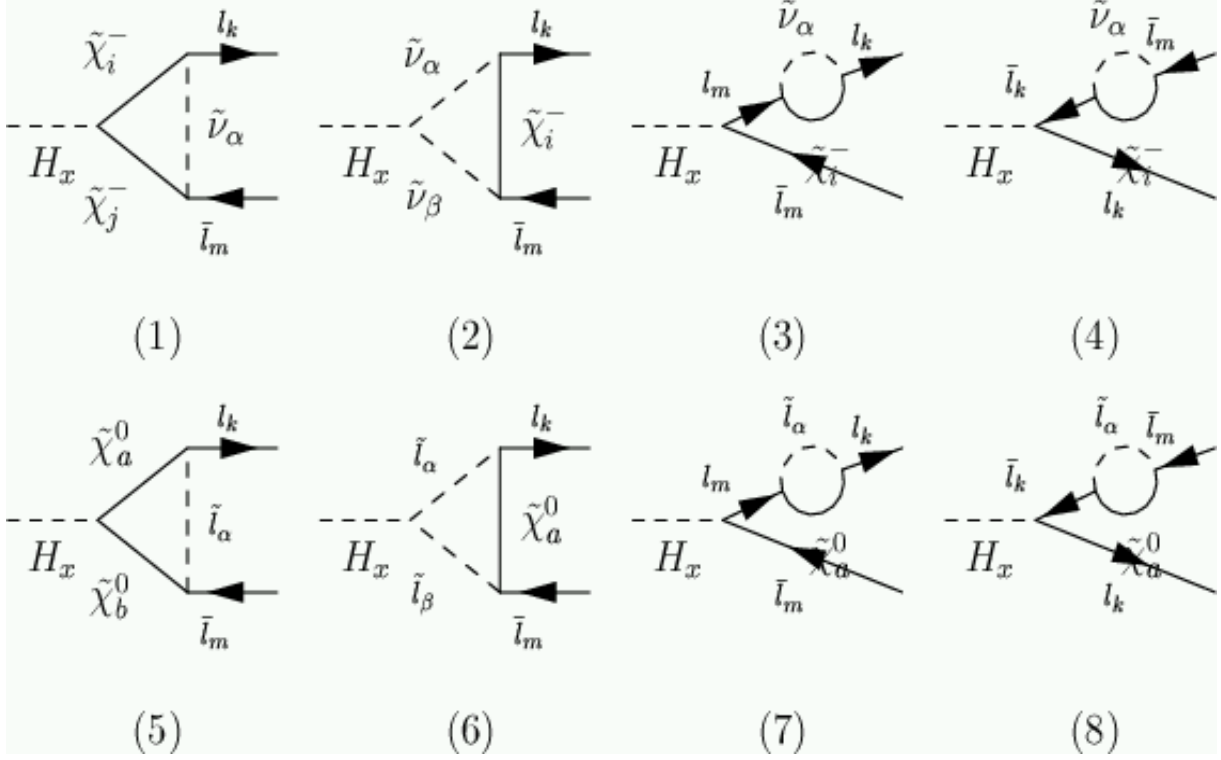


FIG. 4: One-loop diagrams for the LFV HD in the M SSM -seesaw model

The results of the branching ratios for the LFV HD, in the  $\tau$  channel, as a function of the Majorana mass,  $m_N$ , in scenario A with degenerate heavy neutrinos, are illustrated in fig. 5, for several  $\tan\beta$  values,  $\tan\beta = 3; 10; 30; 50$ . The explored range in  $m_N$  is from  $10^8$  GeV up to  $10^{14}$  GeV which is favorable for baryogenesis. From this figure we see that the branching ratios for the light Higgs boson are smaller than the heavy Higgs ones in about two orders of magnitude. The ratios of  $H_0$  and  $A_0$  are very similar in all the plots and, for this scenario, can reach values up to  $10^{-6}$  in the region of high  $\tan\beta$ . From these plots, we also see clearly the extremely high sensitivity to  $\tan\beta$  of the LFV HD rates for all Higgs bosons. It is evident as well the mild sensitivity to  $m_N$ . In fact, the dependence with  $m_N$  can only be appreciated at low  $\tan\beta$  values, as can be seen in the plots for  $\tan\beta = 3$ . We understand this behaviour as follows. We have found that the Higgs ratios are dominated at large  $\tan\beta$  by the chargino contributions, that is from the loop diagrams (1),(2),(3) and (4) in fig. 4. For instance, for  $m_N = 10^{14}$  GeV,  $M_0 = 400$  GeV, and  $M_{1-2} = 300$  GeV, we have found the following ratios between the chargino and neutralino contributions to the  $H^0$  form factors:  $\tilde{F}_L = \tilde{F}_L^0$  for  $j = 1, 2, 14, 178, 1646$  for  $\tan\beta = 3, 10, 30, 50$  respectively, where we have used a

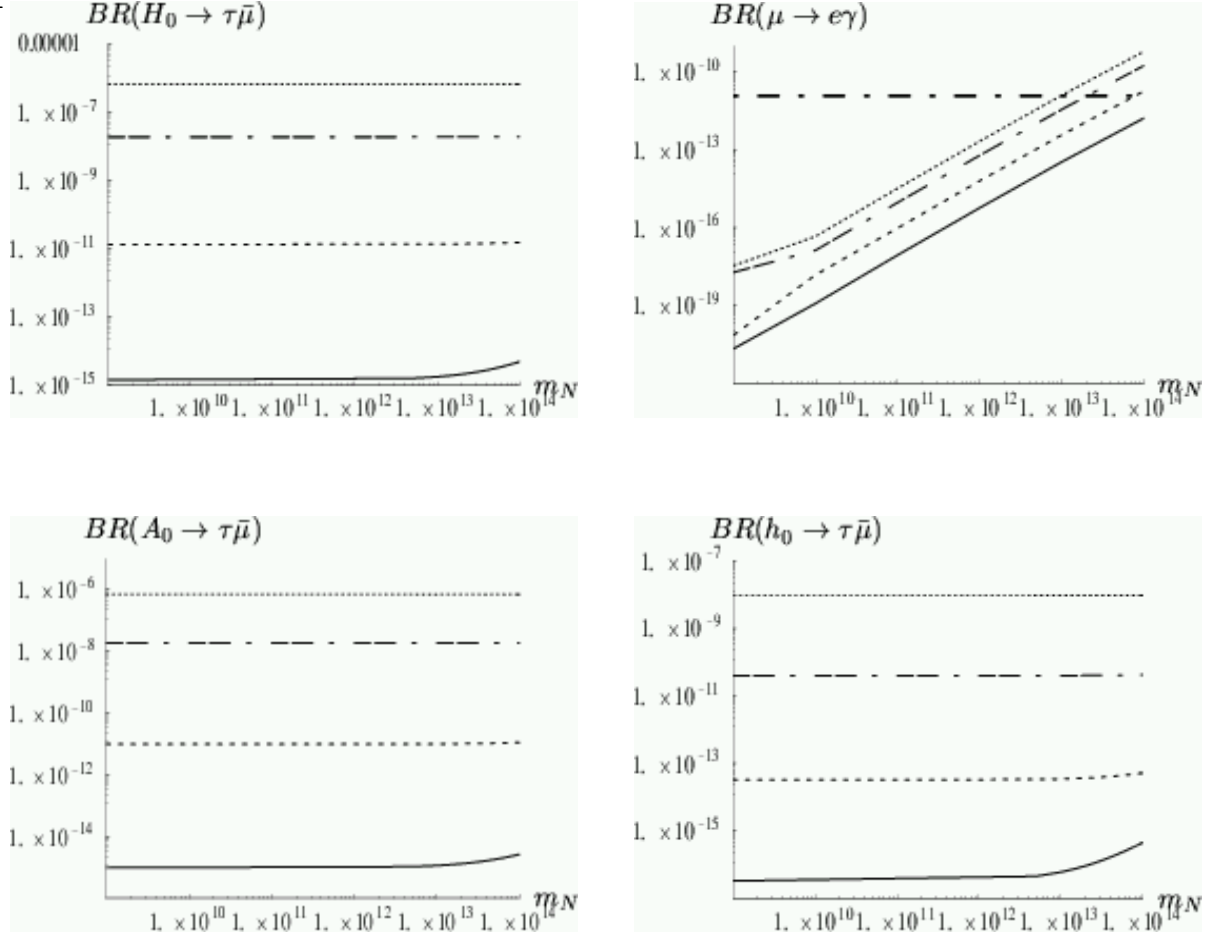


FIG. 5: Dependence of  $BR(H_x \rightarrow \tau \bar{\mu})$  (5a, 5c) and  $BR(\mu \rightarrow e \gamma)$  (5b, 5d) with  $m_N$  (GeV) in scenario A with degenerate neutrinos and real  $R$ , for several values of  $\tan \beta$ . (5a) Upper-left panel,  $H_x = H_0$ , (5c) lower-left panel,  $H_x = A_0$  and (5d) lower-right panel,  $H_x = h_0$ . (5b) Upper-right panel: Dependence of  $BR(\mu \rightarrow e \gamma)$  with  $m_N$  for several values of  $\tan \beta$ . In all plots, the solid, dashed, dashed-dotted and dotted lines are the predictions for  $\tan \beta = 3; 10; 30$  and  $50$ , respectively. The horizontal line in (5b) is the upper experimental bound on  $BR(\mu \rightarrow e \gamma)$ . The other input parameters are,  $M_0 = 400$  GeV,  $M_{1=2} = 300$  GeV and  $A_0 = 0$ .

simplified notation,  $\tilde{F_L} = F_{L,H_0}^{(1)} + F_{L,H_0}^{(2)} + F_{L,H_0}^{(3)} + F_{L,H_0}^{(4)}$ ,  $\tilde{F_L}^0 = F_{L,H_0}^{(5)} + F_{L,H_0}^{(6)} + F_{L,H_0}^{(7)} + F_{L,H_0}^{(8)}$ . Similar  $\sim \sim^0$  ratios are found for the corresponding  $F_R$  form factors. The relative ratio found of  $F_L = F_R = 17$  is nicely explained by the  $m_L = m_R$  ratio. For the lightest Higgs boson, we find  $\tilde{F_L} = \tilde{F_L}^0$  for  $j = 0.4; 4; 41; 300$  correspondingly.

Regarding the comparative size of the contributions from the various chargino loop diagrams we have found that, at large  $\tan \beta$  the external legs corrections are clearly the

dom inant ones. Concretely, for  $j(F_{L,H_0}^{(3)} + F_{L,H_0}^{(4)}) = F_L \sim j, F_{L,H_0}^{(1)} = F_L \sim j$  and  $F_{L,H_0}^{(2)} = F_L \sim j$  we get the respective percentages, 60.9%, 39% and 0.1%, for  $\tan \theta = 10$  and 93.8%, 6.2%, 0% for  $\tan \theta = 50$ . This dominance of the external legs corrections explains the high sensitivity of the LFV HD rates to  $\tan \theta$ . The contributions of these diagrams to the  $H^0$  form factors grow as  $(\tan \theta)^3$ , and there is no cancellation of GIM type when summing over the three sneutrino species in the internal propagators, because of the non-degeneracy in their masses. This absence of GIM-like cancellations is a well known fact in softly broken SUSY theories. The crucial point here is that, after the running down to the low energies, the sneutrino masses are not degenerate any more, and the effect of this difference is magnified by the non-vanishing of the off-diagonal  $U_{MNS}^{ij}$  factors in the couplings, specially by  $U_{MNS}^{23}$ , which in our scenario is maximal,  $U_{MNS}^{23} = 0.707$ . This dominance occurs for all the explored  $m_N$  values, and can be translated, following the previously introduced terminology of  $U_{MNS}$  versus misalignment effects, into the evident dominance of the first over the second ones, for  $\tan \theta$  values above 10. This also explains the very mild dependence with  $m_N$ , since it only enters via the  $U_{MNS}^{ij}$ , and these effects are overwhelmed by the  $U_{MNS}$  effects.

The comparative role of the two mentioned sources of flavor changing in these Higgs boson decays can be more clearly seen in Fig. 6. Here we show the predictions for  $BR(H_0 \rightarrow l^+ l^-)$  as a function of  $\theta_{23}$  in a generic MSSM scenario where the  $U_{MNS}^{ij}$  parameters are not predicted (as it is done in the seesaw model under study here) but they are considered as free parameters. For simplicity we set here  $\theta_{12} = \theta_{13} = 0$ . The other input values are set to  $\tan \theta = 50, M_0 = 400$  GeV and  $M_{1=2} = 300$  GeV. The solid lines are the branching ratios including both effects, the misalignment effect from  $\theta_{23} \neq 0$  and the  $U_{MNS}$  effect from the input experimental values in eq. 9. The dashed lines are the corresponding predictions by setting  $U_{MNS} = 1$  in the  $U_{MNS}$  couplings. Notice that these dashed lines follow approximately a quadratic dependence with  $\theta_{23}$ , which is the predicted one in the mass insertion approximation. It is also clear from the different behaviour of the solid lines that our assumption of  $U_{MNS} \neq 1$  leads to important differences in the predictions of the branching ratios. In particular, for  $\theta_{23} = 0$ , the ratio  $BR(H_0 \rightarrow l^+ l^-) = 7 \times 10^{-7}$  is exclusively produced from the experimental  $U_{MNS}$  input.

The obvious conclusion from this plot that the  $U_{MNS}$  effect is very important. The corresponding plots for lower values of  $\tan \theta$  (not shown here) manifest a similar qualitative behaviour of the two competing lepton flavor changing sources. The difference is just the crossing of the two lines which occurs instead at much lower  $\theta_{23}$  values of the order of

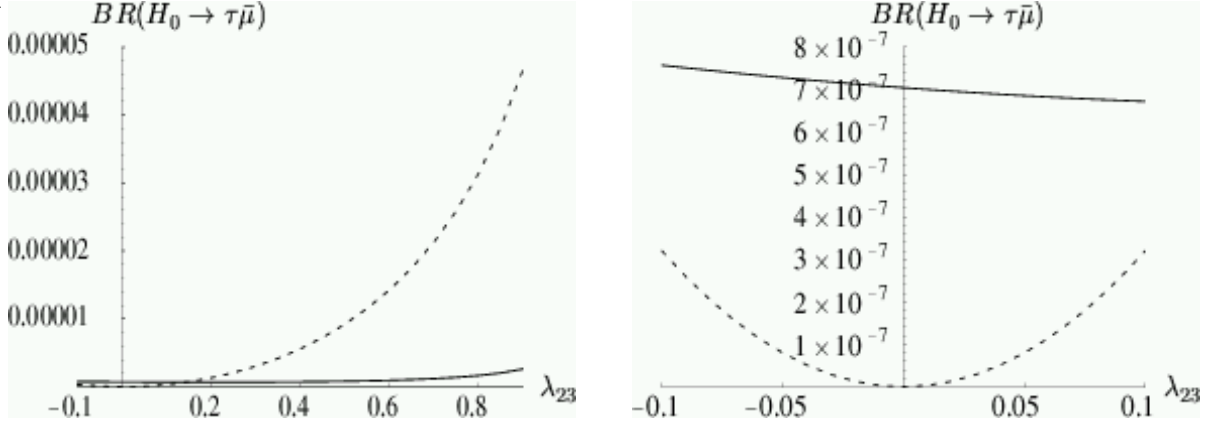


FIG. 6: (6a) Left panel: Dependence of the BR ( $H_0 \rightarrow \tau \bar{\mu}$ ) with  $\lambda_{23}$  for  $\tan \theta = 50$ . Solid lines are for  $U_{M_N S}$  fixed to the experimental data, as given in the text. Dashed lines are for  $U_{M_N S}$  fixed to the identity matrix in the chargino couplings. (6b) Right panel: The same as in (6a) for the  $-0.1 < \lambda_{23} < 0.1$  region. The input parameters are  $\lambda_{12} = \lambda_{13} = 0$ ,  $M_0 = 400$  GeV,  $M_{1=2} = 300$  GeV and  $A_0 = 0$ . The other parameters, got from mSUSPECT [20], are  $\lambda = 385$  GeV,  $m_{H_0} = 340$  GeV.

$10^{-4}$ . This fig. 6 also illustrates that for large  $\lambda_{23}$  values and if one neglects the  $U_{M_N S}$  effects, the predicted branching ratios can be very large. For instance, for  $\lambda_{23} = 0.8$  we get  $BR(H_0 \rightarrow \tau \bar{\mu}) = 3 \times 10^{-5}$  which is in agreement with the results of ref. [12]. Larger branching ratios can be got for lower values of  $M_0$  and/or  $M_{1=2}$ . In this case, they can reach values up to  $10^{-4}$ , as was already announced in ref. [12]. However, we believe that to neglect the effects from  $U_{M_N S}$  is not justified, accordingly to our discussions above.

Regarding the comparison with the  $H \rightarrow e^+ e^-$  decays, we plot in fig. 5b, our predictions for their branching ratios as a function of  $m_N$ , for the same input values as in the Higgs boson decays. The plot shows the well known quadratic dependence with  $\tan \theta$  and the expected  $m_N$  dependence via the neutrino Yukawa couplings. The horizontal dashed line represents the present experimental upper limit of  $BR(H \rightarrow e^+ e^-) < 1.2 \times 10^{-11}$  [5]. From this plot we conclude that, in order to be in agreement with data, there is a maximum allowed value of  $m_N$  for each choice of  $\tan \theta$ . As the Higgs branching ratios are nearly independent on  $m_N$ , their rates will be constrained just from the maximum allowed  $\tan \theta$  values. For instance, for  $m_N = 8 \times 10^{13}$  GeV, only  $\tan \theta < 10$  are allowed, and the maximum Higgs decay rates that can be got are about  $10^{-11}$ . For  $m_N = 10^{13}$  GeV,  $\tan \theta$  values up to 50 are allowed and the Higgs ratios can reach values up to  $7 \times 10^{-7}$ . Obviously, larger values of these LFV HD

ratios could be got for larger  $\tan \theta$  values, but we have not considered them here.

We have also explored the changes in the predictions for non-vanishing  $\theta_{13}$ , concretely for  $\theta_{13} = 5^\circ$ . We have found that the LFV HD rates are quite insensitive to this parameter, and we have confirmed the high sensitivity of the  $\bar{e} \rightarrow e$  rates to it. For instance, for  $\theta_{13} = 5^\circ$  and  $m_N = 10^{13}$  GeV, the maximum allowed  $\tan \theta$  value is 10, to be compared with 50 in the  $\theta_{13} = 0$  case.

In addition we have studied the dependence of the Higgs ratios in this scenario A with the alternative choice of complex R. For this we use the parametrization given in case 2, and assume for simplicity  $a = b = c$ . We then compute the branching ratios as a function of the  $a$  parameter, for the range  $0 < a < 0.1$ . We compute as well the branching ratios of

$\bar{e} \rightarrow e$  for the same selected parameters and again require compatibility with data. We do not show the plots for this case but comment on the most relevant features. We find that the Higgs ratios are not much sensitive to this parameter, but the  $\bar{e} \rightarrow e$  rates increase notably with it and overpass the experimental limit in the large  $m_N$  explored region. We have checked that  $\tan \theta = 50$  is allowed for values as low as  $m_N = 10^{10}$  GeV. This growing with  $a$  is a clear consequence of the increasing of  $j_{12}$  with this parameter, specially  $j_{12}$  as can be seen in fig. (3).

Regarding the other decays,  $\bar{e} \rightarrow e$  and  $\bar{e} \rightarrow \nu$ , we have checked by explicit computation of the corresponding rates that they are, for all the studied cases in this work, well below the present experimental upper limits of  $BR(\bar{e} \rightarrow e) < 2.7 \times 10^{-6}$  [7] and  $BR(\bar{e} \rightarrow \nu) < 6 \times 10^{-7}$  [6] respectively.

The branching ratios for the Higgs boson decays into  $e$  and  $\nu$  are smaller than the ones, as expected, and we do not show plots for them. For instance, for  $m_N = 10^{14}$  GeV, and  $\tan \theta = 30$  we find  $BR(H^0 \rightarrow e\bar{e}) = 50$  and  $BR(H^0 \rightarrow \nu\bar{\nu}) = 10^6$  respectively.

We next present the results for hierarchical neutrinos, scenario B. The results for real R and complex R are shown in figs. 7 and 8 respectively. We choose in these plots the mass hierarchy  $(m_{N_1}; m_{N_2}; m_{N_3}) = (10^8; 2 \times 10^8; 10^{14})$  GeV, which is one of the possible choices for successful bariogenesis, and use the parametrization of case 1. In fig. 7 we show the dependence with real  $\theta_1$ , and in fig. 8 the dependence with the modulus for complex  $\theta_1$ . In both cases we take,  $\theta_2 = \theta_3 = 0$ .

It is important to notice that in this scenario of hierarchical heavy neutrinos, the pre-

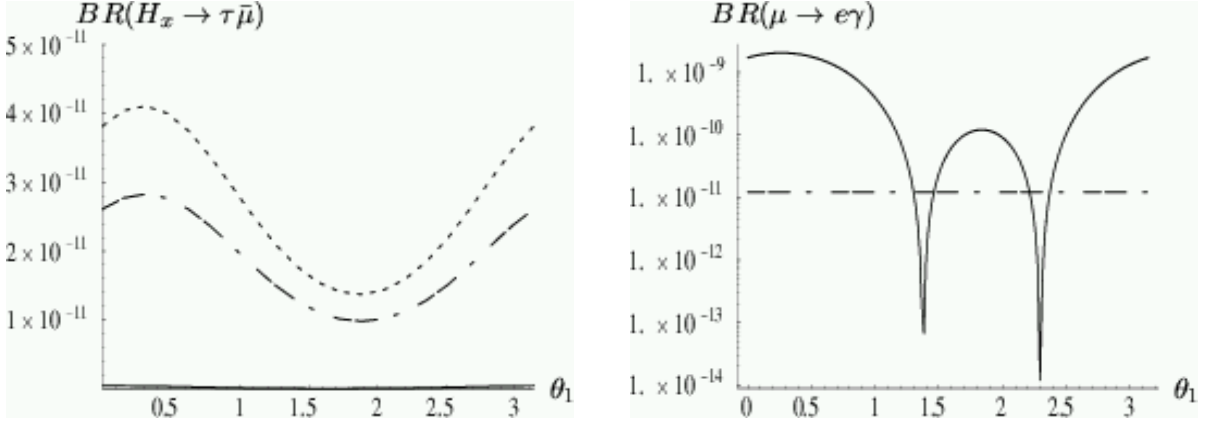


FIG . 7: (7a) Left panel: D ependence of  $BR(H_x \rightarrow \tau \bar{\mu})$  with  $\theta_1$ . Solid, dashed and dashed-dotted lines correspond to  $H_x = (h_0; H_0; A_0)$  respectively. (7b) Right panel: D ependence of  $BR(\mu \rightarrow e\gamma)$  with  $\theta_1$ . Both panels are in scenario B , case 1 for real  $\theta_1$ ,  $(m_{N_1}; m_{N_2}; m_{N_3}) = (10^8; 2 \times 10^8; 10^{14})$  GeV,  $\theta_2 = \theta_3 = 0$ ,  $\tan \theta = 10$ ,  $M_0 = 400$  GeV,  $M_{1=2} = 300$  GeV, and  $A_0 = 0$ .

dition for the  $\mu \rightarrow e\gamma$  decay are much larger than in the case of degenerate neutrinos, in agreement with [8], and therefore the allowed parameter space is more constrained. This can be seen numerically by comparing the values in fig. 5b with the value in fig. 7b with  $\theta_1 = 0$ . The behaviour with real  $\theta_1$  shows that, due to the high rates obtained for  $\mu \rightarrow e\gamma$ , only very low  $\tan \theta$  values are allowed. The plots in this figure are for  $\tan \theta = 10$ , and in this case, compatibility with data occurs only in the very narrow dips. The presence of these narrow regions where the  $\mu \rightarrow e\gamma$  rates are drastically suppressed were already pointed out in ref. [8]. Notice, however, that the localization of these dips and the maxima are placed in different points than in ref. [8]. We have checked that this shift is due to the effects from the  $U_{MNS}$  factors in the chargino couplings, which were not included in ref. [8]. These effects modify the pattern of the branching ratio relative to the expected one from the  $\theta_1$  behaviour with  $\theta_1$  of fig. 3.

For low  $\tan \theta$ , the Higgs ratios show a mild dependence with  $\theta_1$ , as it is illustrated in fig. (7a) for  $\tan \theta = 10$ . For  $\tan \theta > 10$  this dependence is almost unappreciable, due again to the fact that the  $U_{MNS}$  effect dominates. For the allowed values of  $m_N$ ,  $\tan \theta$  and  $\theta_1$ , which in the plot shown in fig. (7b) correspond to the narrow dips, the Higgs rates can only reach small values of up to about  $2 \times 10^{-11}$ . The rates for  $H^0$  and  $A^0$  are very similar and the rates for  $h^0$  are more than two orders of magnitude smaller.

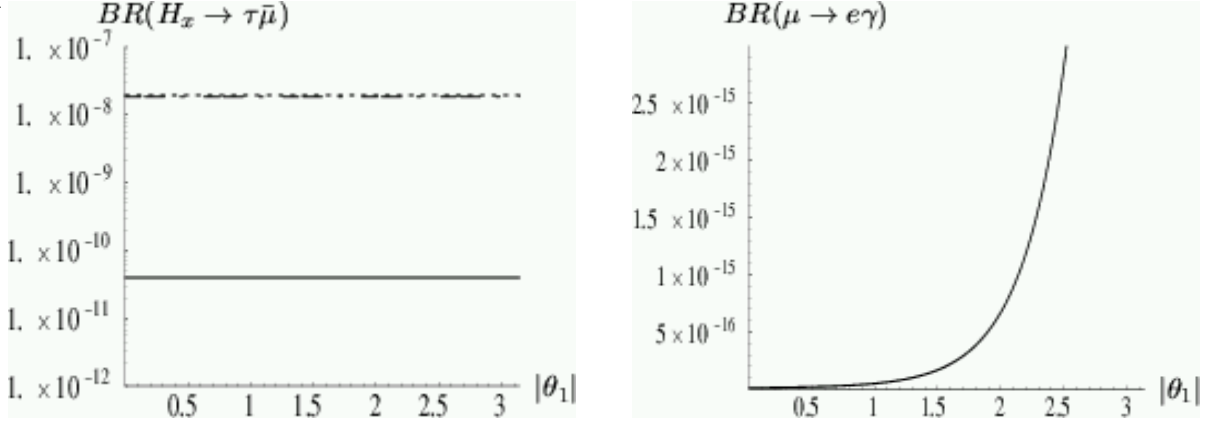


FIG. 8: (8a) Left panel: Dependence of  $BR(H_x \rightarrow \tau \bar{\mu})$  with  $|j_1 j_2|$ . Solid, dashed and dashed-dotted (the two later almost undistinguishable) lines correspond to  $H_x = (h_0; H_0; A_0)$  respectively. (8b) Right panel: Dependence of  $BR(\mu \rightarrow e\gamma)$  with  $|j_1 j_2|$ . Both panels are in scenario B, case 1 for complex  $j_1$ ,  $(m_{N_1}; m_{N_2}; m_{N_3}) = (10^8; 2 \times 10^8; 10^{10})$  GeV,  $\arg(j_1) = \pi/4$ ,  $\theta_2 = \theta_3 = 0$ ,  $\tan \theta_1 = 30$ ,  $M_0 = 400$  GeV,  $M_{1=2} = 300$  GeV, and  $A_0 = 0$ .

Regarding the behaviour with the other angles, we have checked that  $\mu \rightarrow e\gamma$  is very poorly dependent with  $\theta_3$ , but the rates exceed the experimental upper limit in all the explored cases. We have not studied the dependence of the Higgs rates with this parameter. The qualitative behaviour of the Higgs rates with  $\theta_2$  is quite similar to that of  $\theta_1$ . The behaviour of the  $\mu \rightarrow e\gamma$  rates with  $\theta_2$  are also quite similar to those of  $\theta_1$  but now there is only one deep at about  $\theta_2 = 2$  where there is compatibility with data, instead of the two deeps mentioned before. The Higgs ratios, corresponding to these deeps are again very small.

For complex  $j_1$ , the Higgs ratios can reach larger values, particularly for large  $\tan \theta_1$ . However, the restrictions from  $\mu \rightarrow e\gamma$  are very demanding, and compatibility with data requires lower values of  $m_N$  and/or  $\tan \theta_1$ . The plots in fig (8) illustrate the case of  $\tan \theta_1 = 30$  with a lower mass value for the heaviest neutrino of  $m_N = 10^{10}$  GeV. We see that  $\mu \rightarrow e\gamma$  is perfectly compatible with data, and the corresponding Higgs ratios are three orders of magnitude larger than in the previous case with real  $j_1$  but still small, being about  $2 \times 10^{-8}$ . We believe this could be enhanced by choosing slightly higher values of  $\tan \theta_1$  and/or the heaviest neutrino mass  $m_N$ , but this must be done very finely since, as we have said, the increase in the  $\mu \rightarrow e\gamma$  rates is very sensitive to these parameters.

So far we have fixed the soft mass parameters to the particular values  $M_0 = 300$  GeV,

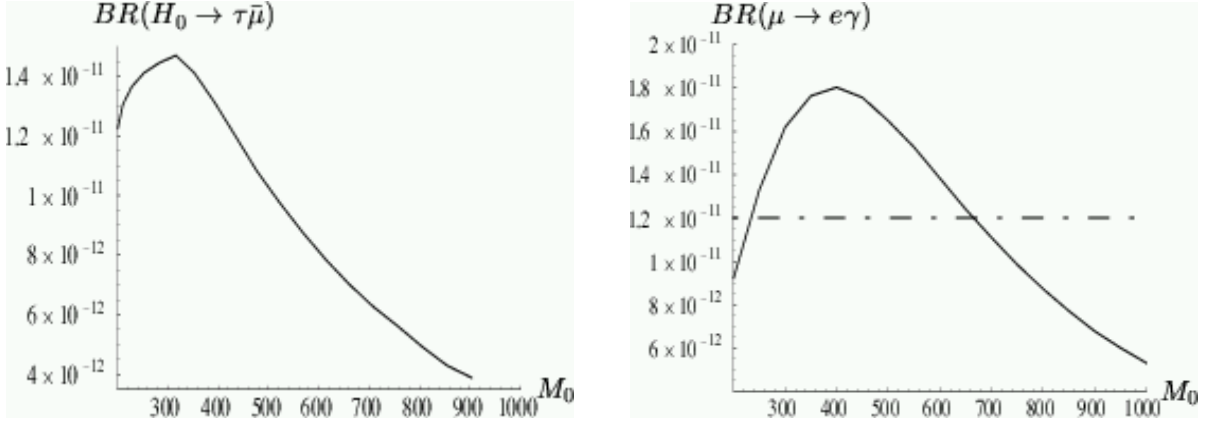


FIG . 9: (9a) Left panel: D ependence of B R ( $H_0 \rightarrow \tau \bar{\mu}$ ) with  $M_0$  (GeV). (9b) Right panel: D ependence of B R ( $\mu \rightarrow e \gamma$ ) with  $M_0$  (GeV). The horizontal line is the upper experimental bound on B R ( $\mu \rightarrow e \gamma$ ). Both gures are in scenario A , case 1, for  $m_N = 10^{14}$  GeV, R real,  $M_{1=2} = 300$  GeV and  $\tan \beta = 10$ .

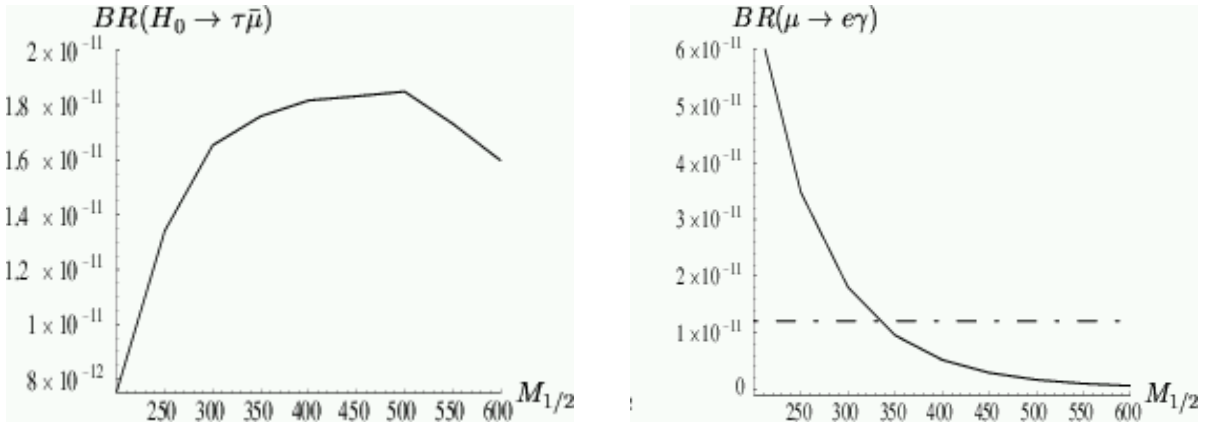


FIG . 10: (10a) Left panel: D ependence of B R ( $H_0 \rightarrow \tau \bar{\mu}$ ) with  $M_{1=2}$  (GeV). (10b) Right panel: D ependence of B R ( $\mu \rightarrow e \gamma$ ) with  $M_{1=2}$  (GeV). The horizontal line is the upper experimental bound on B R ( $\mu \rightarrow e \gamma$ ). Both gures are in scenario A , case 1, for  $m_N = 10^{14}$  GeV, R real,  $M_0 = 400$  GeV and  $\tan \beta = 10$ .

$M_{1=2} = 400$  GeV and  $A_0 = 0$ . As we have said, we do not expect much changes in the LFVHD rates for other choices of  $A_0$ . The dependence of the branching ratios for the  $H^0 \rightarrow \tau \bar{\mu}$  and  $\mu \rightarrow e \gamma$  decays with  $M_0$  and  $M_{1=2}$  are shown in gs. 9 and 10 respectively. The results for  $\mu \rightarrow e \gamma$  show that, for some selected values of  $m_N$  and  $\tan \beta$ , one can find  $M_0$  and  $M_{1=2}$  values above which the rates are well below the experimental limit. For instance, for  $\tan \beta = 10$  and degenerate heavy neutrinos with  $m_N = 10^{14}$  GeV, if  $M_{1=2} = 300$  GeV,

all values above  $M_0 = 680$  GeV give compatible rates with data; and if  $M_0 = 400$  GeV, all values above  $M_{1=2} = 340$  GeV do it as well. Thus, due to the smooth dependence of the LFVHD on these parameters, by taking larger values of  $M_0$  and  $M_{1=2}$  than the ones chosen in all our previous plots we can get larger allowed values of  $\tan\beta$  and therefore larger values of the LFVHD rates. In particular, we see in fig. 10, corresponding to  $\tan\beta = 10$  and  $m_N = 10^{14}$  GeV, that for  $M_0 = 400$  GeV and values of  $M_{1=2}$  between 300 GeV and 600 GeV the Higgs ratios do not change much, whereas the  $H \rightarrow \tau\bar{\mu}$  rates go down in the experimental limit.

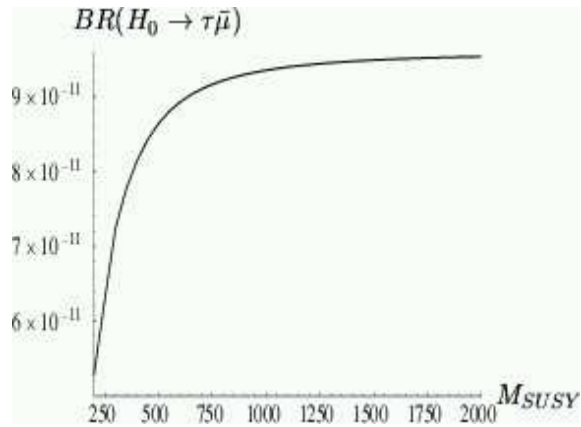


FIG. 11: Behaviour of  $H_0 \rightarrow \tau\bar{\mu}$  as a function of the common SUSY mass,  $M_{\text{SUSY}}$ .  $m_{\tilde{L};1} = m_{\tilde{E};1} = M_0 = M_2$  and  $M_1 = \frac{5}{3} \tan^2\beta M_2$ . Here we fix  $\chi_{23} = 0.01$ ,  $\chi_{12} = \chi_{13} = 0$ ,  $\tan\beta = 50$  and  $m_{H_0} = 340$  GeV.

Finally, we study the behaviour of the LFVHD rates at very large SUSY masses to learn if the SUSY particles participating in the loops do or do not decouple in these decays. For this, we consider a generic MSSM scenario, with the  $\chi_{ij}$  being free parameters, which we fix here to the values  $\chi_{23} = 0.01$ ,  $\chi_{12} = \chi_{13} = 0$  and, for simplicity, we take a common SUSY mass at the electroweak scale,  $M_{\text{SUSY}} = m_{\tilde{L};1} = m_{\tilde{E};1} = M_0 = M_2$  and  $M_1 = \frac{5}{3} \tan^2\beta M_2$ . We show in fig. 11  $\text{BR}(H_0 \rightarrow \tau\bar{\mu})$  as a function of this common SUSY scale, for  $\tan\beta = 50$  and  $m_{H_0} = 340$  GeV. We see clearly that the branching ratio approaches asymptotically to a constant non-vanishing value, of about  $10^{-10}$ , and therefore the charginos, neutralinos, charged sleptons and sneutrinos do not decouple in this observable. This non-decoupling behaviour is in contrast with the behaviour of  $\text{BR}(H \rightarrow \tau\bar{\mu})$ , which scales as  $(M_W/M_{\text{SUSY}})^4$ , and explains the comparatively large LFVHD rates found here.

## V . C O N C L U S I O N S

In this paper we have studied in full detail the lepton flavor violating Higgs boson decays that are produced if the neutrinos get their masses via the seesaw mechanism. We have considered the two most popular seesaw models with three generations, the SM seesaw and the MSSM seesaw. Within the SM seesaw we have found extremely small branching ratios which are explained in terms of the decoupling behaviour of the heavy Majorana neutrinos and the smallness of the light neutrino masses. In the MSSM seesaw we find, in contrast, branching ratios that are many orders of magnitude larger (in fact, more than 40!). The larger ratios found are for  $H_0 \rightarrow \ell^+ \ell^-$  decays. After exploring the dependence of the  $H_0 \rightarrow \ell^+ \ell^-$  decay rates with all the involved parameters of the MSSM seesaw, and by requiring compatibility with data of the correlated predictions for  $H_0 \rightarrow e^+ e^-$  and  $H_0 \rightarrow \mu^+ \mu^-$  decays, we find that  $\text{BR}(H_0 \rightarrow \ell^+ \ell^-)$  as large as  $10^{-6}$  can be reached. These ratios are mostly sensitive to  $\tan \beta$ , which has been taken in the range  $3 < \tan \beta < 50$ , and the largest ratios found in this work are for  $\tan \beta = 50$ . Larger  $\tan \beta$  values can lead to Higgs ratios closer to the future experimental reach, but we have not tried this because it would require to perform a resummation of the large  $\tan \beta$  contributions that is beyond the scope of this work.

## Acknowledgments

We wish to acknowledge Alberto Casas for valuable discussions. We also thank Ana Teixeira for her help with the usage of the `M SUSPECT` package. D. Temes thank F. Boudjema for useful comments and for reading the manuscript. E. Arganda and A. M. Curiel acknowledge the Spanish Ministry of Science and Education (MEC) for financial support by their FPU grants, AP2003-3776 and AP2001-0678 respectively. This work was supported by the Spanish MEC under project FPA2003-04597.

## A P P E N D I X A

We present here the analytical results for the form factors in the SM seesaw, in the Feynman 't Hooft gauge.

$$\begin{aligned}
F_L^{(1)} &= \frac{g^2}{4m_W^3} \frac{1}{16^2} B_{k n_i} B_{k n_j} m_k m_{n_j} (m_{n_i} + m_{n_j}) \text{Re } C_{n_i n_j} + i(m_{n_j} - m_{n_i}) \text{Im } C_{n_i n_j} C_0 \\
&+ (C_{12} - C_{11}) (m_{n_i} + m_{n_j}) \text{Re } C_{n_i n_j} m_{\frac{3}{4}k} m_{n_j} m_{n_i} m_{\frac{1}{4}k}^2 + m_{n_i} m_{n_j}^2 m_{\frac{1}{4}k} + m_{n_i}^2 m_{n_j} m_{\frac{1}{4}k} \\
&+ i(m_{n_j} - m_{n_i}) \text{Im } C_{n_i n_j} m_{\frac{3}{4}k} m_{n_j} + m_{n_i} m_{\frac{1}{4}k} m_{\frac{1}{4}k}^2 m_{n_i} m_{n_j}^2 m_{\frac{1}{4}k} + m_{n_i}^2 m_{n_j} m_{\frac{1}{4}k} \\
F_R^{(1)} &= \frac{g^2}{4m_W^3} \frac{1}{16^2} B_{k n_i} B_{k n_j} m_{n_i} m_{\frac{1}{4}k} (m_{n_i} + m_{n_j}) \text{Re } C_{n_i n_j} i(m_{n_j} - m_{n_i}) \text{Im } C_{n_i n_j} C_0 \\
&+ C_{12} (m_{n_i} + m_{n_j}) \text{Re } C_{n_i n_j} m_{\frac{3}{4}k} m_{n_i} m_{n_i} m_{n_j}^2 m_{\frac{1}{4}k} m_{n_i}^2 m_{n_j} m_{\frac{1}{4}k} + m_{n_j} m_{\frac{1}{4}k}^2 m_{\frac{1}{4}k} \\
&+ i(m_{n_j} - m_{n_i}) \text{Im } C_{n_i n_j} m_{\frac{3}{4}k} m_{n_i} + m_{n_i} m_{n_j}^2 m_{\frac{1}{4}k} m_{n_i}^2 m_{n_j} m_{\frac{1}{4}k} + m_{n_j} m_{\frac{1}{4}k}^2 m_{\frac{1}{4}k}
\end{aligned}$$

where  $C_{11;12} = C_{11;12} (m_{\frac{1}{4}k}^2; m_H^2; m_W^2; m_{n_i}^2; m_{n_j}^2)$  and  $C_0 = C_0 (m_{\frac{1}{4}k}^2; m_H^2; m_W^2; m_{n_i}^2; m_{n_j}^2)$ .

$$\begin{aligned}
F_L^{(2)} &= \frac{g^2}{2m_W} \frac{1}{16^2} B_{k n_i} B_{k n_j} m_{\frac{1}{4}k} m_{n_j} (m_{n_i} + m_{n_j}) \text{Re } C_{n_i n_j} + i(m_{n_j} - m_{n_i}) \text{Im } C_{n_i n_j} C_0 \\
&+ (C_{12} - C_{11}) (m_{n_i} + m_{n_j})^2 \text{Re } C_{n_i n_j} + i(m_{n_j} - m_{n_i})^2 \text{Im } C_{n_i n_j} \\
F_R^{(2)} &= \frac{g^2}{2m_W} \frac{1}{16^2} B_{k n_i} B_{k n_j} m_{\frac{1}{4}k} m_{n_i} (m_{n_i} + m_{n_j}) \text{Re } C_{n_i n_j} i(m_{n_j} - m_{n_i}) \text{Im } C_{n_i n_j} C_0 \\
&+ C_{12} (m_{n_i} + m_{n_j})^2 \text{Re } C_{n_i n_j} + i(m_{n_j} - m_{n_i})^2 \text{Im } C_{n_i n_j}
\end{aligned}$$

where  $C_{0;11;12} = C_{0;11;12} (m_{\frac{1}{4}k}^2; m_H^2; m_W^2; m_{n_i}^2; m_{n_j}^2)$ .

$$\begin{aligned}
F_L^{(3)} &= \frac{g^2}{16^2} B_{k n_i} B_{k n_i} m_{\frac{1}{4}k} m_W (C_{11} - C_{12}) \\
F_R^{(3)} &= \frac{g^2}{16^2} B_{k n_i} B_{k n_i} m_{\frac{1}{4}k} m_W C_{12}
\end{aligned}$$

where  $C_{11;12} = C_{11;12} (m_{\frac{1}{4}k}^2; m_H^2; m_W^2; m_{n_i}^2; m_{n_j}^2)$ .

$$\begin{aligned}
F_L^{(4)} &= \frac{g^2}{4m_W} \frac{1}{16^2} B_{k n_i} B_{k n_i} m_{\frac{1}{4}k} m_{\frac{1}{4}k}^2 (C_{12} - 2C_{11}) + m_{n_i}^2 (C_{11} - C_{12}) m_{n_i}^2 C_0 \\
F_R^{(4)} &= \frac{g^2}{4m_W} \frac{1}{16^2} B_{k n_i} B_{k n_i} m_{\frac{1}{4}k}^n C_0 + 2m_{\frac{1}{4}k}^2 C_{11} + m_{n_i}^2 C_{12} + (m_{\frac{1}{4}k}^2 - 2m_H^2) (C_{11} - C_{12}) + 2m_{n_i}^2 C_0
\end{aligned}$$

where  $C_{0;11;12} = C_{0;11;12} (m_{\frac{1}{4}k}^2; m_H^2; m_{n_i}^2; m_W^2; m_W^2)$  and  $C_0 = C_0 (m_{\frac{1}{4}k}^2; m_H^2; m_{n_i}^2; m_W^2; m_W^2)$ .

$$\begin{aligned}
F_L^{(5)} &= \frac{g^2}{4m_W} \frac{1}{16^2} B_{k n_i} B_{k n_i} m_{\frac{1}{4}k}^n C_0 + 2m_{n_i}^2 C_0 + (m_{n_i}^2 + 2m_{\frac{1}{4}k}^2) C_{11} + (m_{\frac{1}{4}k}^2 - m_{n_i}^2 - 2m_H^2) C_{12} \\
F_R^{(5)} &= \frac{g^2}{4m_W} \frac{1}{16^2} B_{k n_i} B_{k n_i} m_{\frac{1}{4}k} m_{n_i}^2 C_0 + m_{\frac{1}{4}k}^2 C_{11} + (m_{\frac{1}{4}k}^2 - m_{n_i}^2) C_{12}
\end{aligned}$$

where  $C_{0;11;12} = C_{0;11;12} (m_{\text{L}}^2; m_{\text{H}}^2; m_{n_i}^2; m_{\text{W}}^2; m_{\text{W}}^2)$  and  $C_0 = C_0 (m_{\text{L}}^2; m_{\text{H}}^2; m_{n_i}^2; m_{\text{W}}^2; m_{\text{W}}^2)$ .

$$F_L^{(6)} = \frac{g^2}{4m_{\text{W}}^3} \frac{1}{16^2} B_{\text{L}n_i} B_{\text{L}n_i} m_{\text{L}} m_{\text{H}}^2 - m_{n_i}^2 (C_0 + C_{11}) + (m_{\text{L}}^2 - m_{n_i}^2) C_{12}$$

$$F_R^{(6)} = \frac{g^2}{4m_{\text{W}}^3} \frac{1}{16^2} B_{\text{L}n_i} B_{\text{L}n_i} m_{\text{L}} m_{\text{H}}^2 - m_{n_i}^2 (C_0 + C_{12}) + m_{\text{L}}^2 (C_{11} - C_{12})$$

where  $C_{0;11;12} = C_{0;11;12} (m_{\text{L}}^2; m_{\text{H}}^2; m_{n_i}^2; m_{\text{W}}^2; m_{\text{W}}^2)$ .

$$F_L^{(7)} = \frac{g^2}{2m_{\text{W}}} \frac{1}{16^2} B_{\text{L}n_i} B_{\text{L}n_i} \frac{m_{\text{L}}^2 m_{\text{L}}}{m_{\text{L}}^2 m_{\text{L}}^2} B_1$$

$$F_R^{(7)} = \frac{g^2}{2m_{\text{W}}} \frac{1}{16^2} B_{\text{L}n_i} B_{\text{L}n_i} \frac{m_{\text{L}}^2 m_{\text{L}}}{m_{\text{L}}^2 m_{\text{L}}^2} B_1$$

$$F_L^{(8)} = \frac{g^2}{4m_{\text{W}}^3} \frac{1}{16^2} B_{\text{L}n_i} B_{\text{L}n_i} \frac{m_{\text{L}}}{m_{\text{L}}^2 m_{\text{L}}^2} - m_{\text{L}}^2 (m_{\text{L}}^2 + m_{n_i}^2) B_1 + 2m_{n_i}^2 m_{\text{L}}^2 B_0$$

$$F_R^{(8)} = \frac{g^2}{4m_{\text{W}}^3} \frac{1}{16^2} B_{\text{L}n_i} B_{\text{L}n_i} \frac{m_{\text{L}}}{m_{\text{L}}^2 m_{\text{L}}^2} - m_{\text{L}}^2 (m_{\text{L}}^2 + m_{n_i}^2) B_1 + m_{n_i}^2 (m_{\text{L}}^2 + m_{\text{L}}^2) B_0$$

where  $B_{0;1} = B_{0;1} (m_{\text{L}}^2; m_{n_i}^2; m_{\text{W}}^2)$ .

$$F_L^{(9)} = \frac{g^2}{2m_{\text{W}}} \frac{1}{16^2} B_{\text{L}n_i} B_{\text{L}n_i} \frac{m_{\text{L}}^2 m_{\text{L}}}{m_{\text{L}}^2 m_{\text{L}}^2} B_1$$

$$F_R^{(9)} = \frac{g^2}{2m_{\text{W}}} \frac{1}{16^2} B_{\text{L}n_i} B_{\text{L}n_i} \frac{m_{\text{L}}^2 m_{\text{L}}}{m_{\text{L}}^2 m_{\text{L}}^2} B_1$$

$$F_L^{(10)} = \frac{g^2}{4m_{\text{W}}^3} \frac{1}{16^2} B_{\text{L}n_i} B_{\text{L}n_i} \frac{m_{\text{L}}}{m_{\text{L}}^2 m_{\text{L}}^2} - m_{\text{L}}^2 (m_{\text{L}}^2 + m_{n_i}^2) B_1 + m_{n_i}^2 (m_{\text{L}}^2 + m_{\text{L}}^2) B_0$$

$$F_R^{(10)} = \frac{g^2}{4m_{\text{W}}^3} \frac{1}{16^2} B_{\text{L}n_i} B_{\text{L}n_i} \frac{m_{\text{L}}}{m_{\text{L}}^2 m_{\text{L}}^2} - m_{\text{L}}^2 (m_{\text{L}}^2 + m_{n_i}^2) B_1 + 2m_{n_i}^2 m_{\text{L}}^2 B_0$$

where  $B_{0;1} = B_{0;1} (m_{\text{L}}^2; m_{n_i}^2; m_{\text{W}}^2)$ .

$$C_0 (p_2^2; p_1^2; m_1^2; m_2^2; m_3^2) - B_0 (p_1^2; m_2^2; m_3^2) + m_1^2 C_0 (p_2^2; p_1^2; m_1^2; m_2^2; m_3^2)$$

In all the previous formulas, summation over all indices are understood. These run as  $i, j = 1; \dots; 6$  for neutrinos, and  $k, m = 1; \dots; 3$ , for charged leptons.

## A P P E N D I X B

### 1. Couplings in the M SSM -seesaw

We present here the coupling factors entering in the M SSM -seesaw formulas.

$$\begin{aligned}
A_{L_j}^{(e; ; )} &= \frac{p \frac{m_e; ; }{2m_w \cos h}}{h} U_{j2}^{(1)} R_1^{(1;2;3)1} + R_2^{(1)} U_{M_N S}^{(1;2;3)2} + R_3^{(1)} U_{M_N S}^{(1;2;3)3} \\
A_R^{(e; ; )} &= V_{j1} R_1^{(1)} U_{M_N S}^{(1;2;3)1} + R_2^{(1)} U_{M_N S}^{(1;2;3)2} + R_3^{(1)} U_{M_N S}^{(1;2;3)3} \\
B_L^{(e; ; )} &= \frac{p}{2} \frac{m_e; ; }{2m_w \cos h} N_{a3} R_{(1;3;5)}^{(1)} + \sin_w N_{a1}^0 \frac{\sin^2_w}{\cos_w} N_{a2}^0 R_{(2;4;6)}^{(1)} \\
B_R^{(e; ; )} &= \frac{p}{2} \sin_w N_{a1}^0 \frac{1}{\cos_w} \left( \frac{1}{2} \sin^2_w \right) N_{a2}^0 R_{(1;3;5)}^{(1)} + \frac{m_e; ; }{2m_w \cos h} N_{a3} R_{(2;4;6)}^{(1)} \\
W_{Lij}^{(x)} &= \frac{1}{2} \left( {}_1^{(x)} U_{j2} V_{i1} + {}_2^{(x)} U_{j1} V_{i2} \right) ; W_{Rij}^{(x)} = \frac{1}{2} \left( {}_1^{(x)} U_{i2} V_{j1} + {}_2^{(x)} U_{i1} V_{j2} \right) \\
D_{Lab}^{(x)} &= \frac{1}{2 \cos_w h} \left( \sin_w N_{b1} - \cos_w N_{b2} \right) \left( {}_1^{(x)} N_{a3} + {}_2^{(x)} N_{a4} \right) \\
&+ \left( \sin_w N_{a1} - \cos_w N_{a2} \right) \left( {}_1^{(x)} N_{b3} + {}_2^{(x)} N_{b4} \right) ; D_{Rab}^{(x)} = D_{Lab}^{(x)} \\
S_{L;1}^{(x)} &= \frac{m_1}{2m_w \cos h} {}_1^{(x)} ; S_{R;1}^{(x)} = S_{L;1}^{(x)} \\
g_{H_{xx}^{\pm} \mp}^{(x)} &= ig g_{LL;e}^{(x)} R_1^{(1)} R_1^{(1)} + g_{RR;e}^{(x)} R_2^{(1)} R_2^{(1)} + g_{LR;e}^{(x)} R_1^{(1)} R_2^{(1)} + g_{RL;e}^{(x)} R_2^{(1)} R_1^{(1)} \\
&+ g_{LL;e}^{(x)} R_3^{(1)} R_3^{(1)} + g_{RR;e}^{(x)} R_4^{(1)} R_4^{(1)} + g_{LR;e}^{(x)} R_3^{(1)} R_4^{(1)} + g_{RL;e}^{(x)} R_4^{(1)} R_3^{(1)} \\
&+ g_{LL;e}^{(x)} R_5^{(1)} R_5^{(1)} + g_{RR;e}^{(x)} R_6^{(1)} R_6^{(1)} + g_{LR;e}^{(x)} R_5^{(1)} R_6^{(1)} + g_{RL;e}^{(x)} R_6^{(1)} R_5^{(1)} \\
g_{H_{x\sim}^{\pm} \sim} &= ig g_{LL;e}^{(x)} R_1^{(\pm)} R_1^{(\pm)} + g_{RR;e}^{(x)} R_2^{(\pm)} R_2^{(\pm)} + g_{LR;e}^{(x)} R_3^{(\pm)} R_3^{(\pm)} \\
g_{LL;1}^{(x)} &= \frac{M_z}{\cos_w} {}_3^{(x)} \frac{1}{2} \sin^2_w + \frac{m_1^2}{M_w \cos h} {}_4^{(x)} \\
g_{RR;1}^{(x)} &= \frac{M_z}{\cos_w} {}_3^{(x)} \sin^2_w + \frac{m_1^2}{M_w \cos h} {}_4^{(x)} \\
g_{LR;1}^{(x)} &= {}_1^{(x)} A_1 {}_5^{(x)} \frac{m_1}{2M_w \cos h} ; g_{RL;1}^{(x)} = g_{LR;1}^{(x)} \\
g_{LL;3}^{(x)} &= \frac{M_z}{2 \cos_w} {}_3^{(x)} \\
&\quad \begin{array}{ccccccccc} 0 & 1 & 0 & 1 & 0 & 1 \\ \hline \sin & \cos & \cos & \sin & \sin & \cos \\ \frac{B}{B} & \frac{B}{B} \end{array} \\
&\quad \begin{array}{c} \sin( + ) \\ \frac{C}{C} \end{array} \\
&\quad \begin{array}{c} \cos( + ) \\ \frac{C}{C} \end{array} \\
&\quad \begin{array}{c} 0 \\ \frac{C}{C} \end{array} \\
\text{where } {}_1^{(x)} &= \frac{B}{B} \sin \frac{C}{C} ; {}_2^{(x)} = \frac{B}{B} \cos \frac{C}{C} ; {}_3^{(x)} = \frac{B}{B} \cos( + ) \frac{C}{C} \\
&\quad \begin{array}{c} i \sin \\ \frac{A}{A} \end{array} \quad \begin{array}{c} i \cos \\ \frac{A}{A} \end{array} \quad \begin{array}{c} 0 \\ \frac{A}{A} \end{array}
\end{aligned}$$

$$\begin{array}{ccc}
0 & 1 & 0 & 1 & 0 & 1 \\
& \sin & & \cos & & h^0 \\
& \frac{B}{B} & \frac{C}{C} & \frac{B}{B} & \frac{C}{C} & \frac{C}{C} \\
\text{and } \frac{(x)}{4} = & \frac{B}{B} \cos & \frac{C}{C} ; & \frac{(x)}{5} = & \frac{B}{B} \sin & \frac{C}{C} ; \text{ for } x = \frac{B}{B} H^0 & \text{respectively.} \\
& \frac{A}{A} & & \frac{A}{A} & & \frac{A}{A} \\
& 0 & & i \cos & & A^0
\end{array}$$

The matrices that rotate to the mass eigenstate basis are:  $U$  and  $V$  for charginos,  $N$  for neutralinos,  $R^{(1)}$  for charged sleptons and  $R^{(2)}$  for sneutrinos.  $U, V$  and  $N$  are taken from ref. [23],  $N_{a1}^0 = N_{a1} \cos \omega + N_{a2} \sin \omega$ ,  $N_{a2}^0 = -N_{a1} \sin \omega + N_{a2} \cos \omega$ , and  $R^{(1)}$  and  $R^{(2)}$  are computed here by the diagonalization procedure presented in section IV. The various indices in the previous formulas run as follows:  $i, j = 1, 2$  for charginos,  $a, b = 1, \dots, 4$  for neutralinos,  $i = 1, \dots, 6$  for charged sleptons,  $i = 1, \dots, 3$  for sneutrinos, and  $l = e, \mu$  for charged leptons. Summation over all indices is understood.

## 2. Form factors in the M SSM -seesaw

We present here the analytical results for the form factors in the M SSM -seesaw.

$$\begin{aligned}
F_{Lx}^{(1)} &= \frac{g^2}{16^2} h \left[ B_0 + m_{\tilde{L}}^2 C_0 + m_{\tilde{L}}^2 C_{12} + m_{\tilde{L}}^2 (C_{11} - C_{12}) \frac{x; \sim}{L1} \right. \\
&\quad + m_{\tilde{L}} m_{\tilde{L}} (C_{11} + C_0) \frac{x; \sim}{L2} + m_{\tilde{L}} m_{\sim j} (C_{11} - C_{12} + C_0) \frac{x; \sim}{L3} + m_{\tilde{L}} m_{\sim j} C_{12} \frac{x; \sim}{L4} \\
&\quad + m_{\tilde{L}} m_{\sim i} (C_{11} - C_{12}) \frac{x; \sim}{L5} + m_{\tilde{L}} m_{\sim i} (C_{12} + C_0) \frac{x; \sim}{L6} + m_{\sim i} m_{\sim j} C_0 \frac{x; \sim}{L7} \left. \right] \\
F_{Lx}^{(2)} &= \frac{ig g_{Hx} \sim \sim}{16^2} \left[ m_{\tilde{L}} (C_{11} - C_{12}) \frac{x; \sim}{L1} - m_{\tilde{L}} C_{12} \frac{x; \sim}{L2} + m_{\sim i} C_0 \frac{x; \sim}{L3} \right] \\
F_{Lx}^{(3)} &= \frac{S_{L \tilde{L}}^{(x)}}{m_{\tilde{L}}^2 m_{\tilde{L}}^2} h \left[ m_{\tilde{L}}^2 \tilde{R} (\tilde{m}_{\tilde{L}}^2) + m_{\tilde{L}}^2 \tilde{R}_s (\tilde{m}_{\tilde{L}}^2) + m_{\tilde{L}} m_{\tilde{L}} \tilde{R} (\tilde{m}_{\tilde{L}}^2) + m_{\tilde{L}} \tilde{L}_s (\tilde{m}_{\tilde{L}}^2) \right] \\
F_{Lx}^{(4)} &= \frac{S_{L \tilde{L}}^{(x)}}{m_{\tilde{L}}^2 m_{\tilde{L}}^2} h \left[ m_{\tilde{L}}^2 \tilde{L} (\tilde{m}_{\tilde{L}}^2) + m_{\tilde{L}} m_{\tilde{L}} \tilde{R}_s (\tilde{m}_{\tilde{L}}^2) + m_{\tilde{L}} m_{\tilde{L}} \tilde{R} (\tilde{m}_{\tilde{L}}^2) + m_{\tilde{L}} \tilde{L}_s (\tilde{m}_{\tilde{L}}^2) \right] \\
F_{Lx}^{(5)} &= \frac{g^2}{16^2} h \left[ B_0 + m_{\tilde{L}}^2 C_0 + m_{\tilde{L}}^2 C_{12} + m_{\tilde{L}}^2 (C_{11} - C_{12}) \frac{x; \sim^0}{L1} \right. \\
&\quad + m_{\tilde{L}} m_{\tilde{L}} (C_{11} + C_0) \frac{x; \sim^0}{L2} + m_{\tilde{L}} m_{\sim b} (C_{11} - C_{12} + C_0) \frac{x; \sim^0}{L3} + m_{\tilde{L}} m_{\sim b} C_{12} \frac{x; \sim^0}{L4} \\
&\quad + m_{\tilde{L}} m_{\sim a} (C_{11} - C_{12}) \frac{x; \sim^0}{L5} + m_{\tilde{L}} m_{\sim a} (C_{12} + C_0) \frac{x; \sim^0}{L6} + m_{\sim a} m_{\sim b} C_0 \frac{x; \sim^0}{L7} \left. \right] \\
F_{Lx}^{(6)} &= \frac{ig g_{Hx} \tilde{L} \tilde{L}}{16^2} \left[ m_{\tilde{L}} (C_{11} - C_{12}) \frac{x; \sim^0}{L1} - m_{\tilde{L}} C_{12} \frac{x; \sim^0}{L2} + m_{\sim a} C_0 \frac{x; \sim^0}{L3} \right] \\
F_{Lx}^{(7)} &= \frac{S_{L \tilde{L}}^{(x)}}{m_{\tilde{L}}^2 m_{\tilde{L}}^2} h \left[ m_{\tilde{L}}^2 \tilde{R} (\tilde{m}_{\tilde{L}}^2) + m_{\tilde{L}}^2 \tilde{R}_s (\tilde{m}_{\tilde{L}}^2) + m_{\tilde{L}} m_{\tilde{L}} \tilde{R} (\tilde{m}_{\tilde{L}}^2) + m_{\tilde{L}} \tilde{L}_s (\tilde{m}_{\tilde{L}}^2) \right] \\
F_{Lx}^{(8)} &= \frac{S_{L \tilde{L}}^{(x)}}{m_{\tilde{L}}^2 m_{\tilde{L}}^2} h \left[ m_{\tilde{L}}^2 \tilde{L} (\tilde{m}_{\tilde{L}}^2) + m_{\tilde{L}} m_{\tilde{L}} \tilde{R}_s (\tilde{m}_{\tilde{L}}^2) + m_{\tilde{L}} m_{\tilde{L}} \tilde{R} (\tilde{m}_{\tilde{L}}^2) + m_{\tilde{L}} \tilde{L}_s (\tilde{m}_{\tilde{L}}^2) \right]
\end{aligned}$$

where,

$$C_{0;11;12} = \begin{array}{l} \nearrow 8 \\ C_{0;11;12} (m_{\frac{1}{k}}^2; m_{H_x}^2; m_{\sim}^2; m_{\sim_i}^2; m_{\sim_j}^2) \text{ in } F_{L;\bar{x}}^{(1)} \\ \nearrow C_{0;11;12} (m_{\frac{1}{k}}^2; m_{H_x}^2; m_{\sim_i}^2; m_{\sim}^2; m_{\sim}^2) \text{ in } F_{L;\bar{x}}^{(2)} \\ \nearrow C_{0;11;12} (m_{\frac{1}{k}}^2; m_{H_x}^2; m_{\sim}^2; m_{\sim_a}^2; m_{\sim_b}^2) \text{ in } F_{L;\bar{x}}^{(5)} \\ \cdot C_{0;11;12} (m_{\frac{1}{k}}^2; m_{H_x}^2; m_{\sim_a}^2; m_{\sim_i}^2; m_{\sim_i}^2) \text{ in } F_{L;\bar{x}}^{(6)} \end{array}$$

and,

$$\sim(k) = k_L \sim(k^2)P_L + k_R \sim(k^2)P_R + m_{Ls} \sim(k^2)P_L + \sim_{Rs} \sim(k^2)P_R : \quad (B1)$$

The coupling factors and self-energies appearing in the neutralino contributions to the form factors are given by,

$$x; \sim^0 = B_{L_a}^{(L_k)} D_{Rab}^{(x)} B_{R_b}^{(L_k)} \quad x; \sim^0 = B_{R_a}^{(L_k)} B_{R_a}^{(L_k)}$$

$$x; \sim^0 = B_{R_a}^{(L_k)} D_{Lab}^{(x)} B_{L_b}^{(L_k)} \quad x; \sim^0 = B_{L_a}^{(L_k)} B_{L_a}^{(L_k)}$$

$$x; \sim^0 = B_{R_a}^{(L_k)} D_{Lab}^{(x)} B_{R_b}^{(L_k)} \quad x; \sim^0 = B_{L_a}^{(L_k)} B_{R_a}^{(L_k)}$$

$$x; \sim^0 = B_{L_a}^{(L_k)} D_{Rab}^{(x)} B_{L_b}^{(L_k)}$$

$$x; \sim^0 = B_{R_a}^{(L_k)} D_{Rab}^{(x)} B_{R_b}^{(L_k)}$$

$$x; \sim^0 = B_{L_a}^{(L_k)} D_{Lab}^{(x)} B_{L_b}^{(L_k)}$$

$$x; \sim^0 = B_{L_a}^{(L_k)} D_{Lab}^{(x)} B_{R_b}^{(L_k)}$$

$${}_{Ls}^0(k^2) = \frac{g^2}{16^2} B_1(k^2; m_{\sim_a}^2; m_{\sim_i}^2) B_{R_a}^{(L_k)} B_{R_a}^{(L_k)}$$

$$m_{\frac{1}{k}} \sim_{Ls}^0(k^2) = \frac{g^2 m_{\sim_a}^2}{16^2} B_0(k^2; m_{\sim_a}^2; m_{\sim_i}^2) B_{L_a}^{(L_k)} B_{R_a}^{(L_k)} \quad (B2)$$

The coupling factors and self-energies appearing in the chargino contributions to the form factors,  $x; \sim$ ,  $x; \sim$ , and  $\sim$  can be obtained from the previous expressions for  $x; \sim^0$ ,  $x; \sim^0$  and  $\sim^0$  by making the replacements  $m_{\sim_a} \rightarrow m_{\sim_i}$ ,  $m_{\sim_i} \rightarrow m_{\sim}$ ,  $B^{(1)} \rightarrow A^{(1)}$ ,  $D^{(x)} \rightarrow W^{(x)}$ ,  $a \rightarrow i$ , and  $b \rightarrow j$ .

The form factors  $F_{R;\bar{x}}^{(i)}; i=1;:8$  can be got from  $F_{L;\bar{x}}^{(i)}; i=1;:8$  by exchanging the indices L  $\leftrightarrow$  R everywhere.

---

[1] B . T . C leveland et al, *Astrophys. J.* 496 (1998) 505; Y . Fukuda et al. [Kam iokande Collaboration], *Phys. Rev. Lett.* 77 (1996) 1683; V . G avrin, *Nuc. Phys. Proc. Suppl.* 91 (2001) 36; W . H am pel et al, *Phys. lett. B* 447 (1999) 127; M . A ltm ann et al *Phys. lett. B* 490 (2000) 16; Y . Fukuda et al. [Super-K am iokande Collaboration], *Phys. Rev. Lett.* 86 (2001) 5651 and 5656; Q . R .A hm ad et al [SNO Collaboration], *Phys. Rev. Lett.* 87 (2001) 071301 [[arX iv:nucl-ex/0106015](#)]; Q . R .A hm ad et al [SNO Collaboration], *Phys. Rev. Lett.* 89 (2002) 011302 [[arX iv:nucl-ex/0204009](#)]; K .E guchiet al [K am LAND Collaboration], *Phys. Rev. Lett.* 90 (2003) 021802 [[arX iv:hep-ex/0212021](#)].

[2] T . Yanagida, in *Workshop on unified theories*, KEK report 79-18 (1979) 95. M . G ellM ann, P . R am ond, R . Slansky, in *Supergravity* (eds. P . van N ieuwenhuizen and D . Freedm an, N oth Holland, Am sterdam , 1979).

[3] Z .M aki, M .N akagawa and S .Sakata, *Prog. Theor. Phys.* 28 (1962) 870; B .P ontecorvo, *Zh. Eksp. Teor. Fiz.* 33 (1957) 549 and 34 (1958) 247.

[4] A .M .C uriel, M .J .H errero, W .H ollik, F .M erz and S .Penaranda, *Phys. Rev. D* 69 (2004) 075009 [[arX iv:hep-ph/0312135](#)].

[5] M . L .B rooks et al [MEGA Collaboration], *Phys. Rev. Lett.* 83 (1999) 1521 [[arX iv:hep-ex/9905013](#)].

[6] K .Inam i, T .H okue and T .O hshima [BELLE Collaboration], *eConfC* 0209101 (2002) TU11 *Nucl. Phys. Proc. Suppl.* 123 (2003) 82] [[arX iv:hep-ex/0210036](#)].

[7] T .E .Coan et al [CLEO Collaboration], *Phys. Rev. D* 55 (1997) 7291 [[arX iv:hep-ex/9701012](#)].

[8] J .A .C asas and A .I barra, *Nucl. Phys. B* 618 (2001) 171 [[arX iv:hep-ph/0103065](#)].

[9] A .P ilaftsis, *Phys. Lett. B* 285 (1992) 68; J .G .K orner, A .P ilaftsis and K .Schilder, *Phys. Rev. D* 47 (1993) 1080 [[arX iv:hep-ph/9301289](#)].

[10] A .P ilaftsis, Z .*Phys. C* 55 (1992) 275 [[arX iv:hep-ph/9901206](#)].

[11] J .L .D iaz-C ruz and J .J .Toscano, *Phys. Rev. D* 62 (2000) 116005 [[arX iv:hep-ph/9910233](#)].

[12] A .B rignole and A .R ossi, *Phys. Lett. B* 566 (2003) 217 [[arX iv:hep-ph/0304081](#)]; A .B rignole and A .R ossi, [arX iv:hep-ph/0404211](#).

[13] W .G rimus and L .Lavoura, *JHEP* 0011 (2000) 042 [[arX iv:hep-ph/0008179](#)].

[14] M . C . G onzalez-G arcia and C . P ena-G aray, *Phys. Rev. D* 68 (2003) 093003

[arX iv:hep-ph/0306001].

[15] P. H. Chankowski, J. R. Ellis, S. Pokorski, M. Raidal and K. Turzynski, Nucl. Phys. B 690 (2004) 279 [arX iv:hep-ph/0403180].

[16] S. Pascoli, S. T. Petcov and C. E. Yaguna, Phys. Lett. B 564 (2003) 241 [arX iv:hep-ph/0301095].

[17] W. Hollik, in Precision Tests of the Standard Electroweak Model, edited by P. Langacker (World Scientific, Singapore, 1995), pp. 37{116; Fortschr. Phys. 38, 165{260 (1990).

[18] R. Mertig, M. Bohm, A. Denner, Comput. Phys. Commun. 64 (1991) 345; T. Hahn, C. Schappacher, Comput. Phys. Commun. 143 (2002) 54 [arX iv:hep-ph/0105349]; T. Hahn, Comput. Phys. Commun. 140 (2001) 418 [arX iv:hep-ph/0012260]; T. Hahn, M. Perez-Victoria, Comput. Phys. Commun. 118 (1999) 153 [arX iv:hep-ph/9807565].

[19] A. Djouadi, J. Kalinowski and M. Spira, Comput. Phys. Commun. 108 (1998) 56 [arX iv:hep-ph/9704448].

[20] A. Djouadi, J. L. Kneur and G. M. M oultaka, arX iv:hep-ph/0211331.

[21] Y. Grossman and H. E. Haber, Phys. Rev. Lett. 78 (1997) 3438 [arX iv:hep-ph/9702421].

[22] J. Hisano, T. Moroi, K. Tobe and M. Yamaguchi, Phys. Rev. D 53 (1996) 2442 [arX iv:hep-ph/9510309].

[23] J. F. Gunion and H. E. Haber, Nucl. Phys. B 272 (1986) 1 Erratum -ibid. B 402 (1993) 567].